Bull Earthquake Eng (2009) 7:801–834
DOI 10.1007/s10518-009-9104-y

ORIGINAL RESEARCH PAPER

Lateral force distributions for the linear static analysis of base-isolated buildings

Donatello Cardone · Mauro Dolce · Giuseppe Gesualdi

Received: 7 July 2008 / Accepted: 20 January 2009 / Published online: 7 February 2009

Abstract This paper presents a new approach for the evaluation of accurate lateral force distributions for the Linear Static Analysis (LSA) of Base Isolated (BI-) buildings. In essence, the proposed lateral force distributions depend on a factor measuring the degree of non-linearity of the Isolation System (IS) and on the ratio between the effective period of the BI-structure (T_{is}) and the fundamental period of the Fixed Based (FB-) structure (T_{fb}). The proposed approach is fully compatible with the Direct Displacement-Based Design (DDBD) method, recently developed by Priestley and co-workers. The proposed lateral force distributions have been derived from the results of a large number of Nonlinear Time-History Analyses (NTHA), carried out on six numerical models of multi-storey buildings, differing in storey number (3, 5 and 8, respectively) and fundamental period of vibration (from 0.25 to 0.8 s) in the fixed-base configuration. A great variety of Isolation Systems (ISs), characterised by either Elasto-Plastic with Hardening (EPH) or Flag-Shaped (FS) force-displacement behaviour, have been considered in the NTHA. The numerical parameters of the IS models have been varied in such a way as to reproduce the actual mechanical behaviour of the main currently used ISs, including: (i) Lead Rubber Bearings (LRB), (ii) High-Damping Rubber Bearings (HDRB), (iii) Friction Pendulum Bearings (FPB), (iv) combinations of flat Sliding Bearings (SB) and Low-Damping Rubber Bearings (LDRB) and (v) Combinations of flat SB and re-centring devices based on Shape Memory Alloys (SMA). Comparisons between the storey shear forces derived with the proposed method and those obtained from NTHA clearly show the great improvements in the accuracy of LSA predictions, when using the proposed lateral force distributions.

D. Cardone (✉) · G. Gesualdi
DiSGG, University of Basilicata, Potenza, Italy
e-mail: donatello.cardone@unibas.it

M. Dolce
Italian Department of Civil Protection, Rome, Italy

Keywords Base-isolated buildings · Direct displacement-based design · Linear static analysis · Lead rubber bearings · Friction pendulum systems · Flag shaped isolation systems

1 Introduction

The Linear Static Analysis (LSA), also known as Equivalent Static Analysis or Equivalent Linear Analysis (CEN 1998; ICBO 1997; NEHRP 1997; ASCE 2005), is a simple method which is particularly suitable for the analysis and design of Base Isolated (BI-) buildings. It is based on the observation that, in many cases, the response of a BI-building is dominated by its first mode of vibration, in which the horizontal displacements are concentrated at the IS level, while the superstructure moves almost like a rigid body. The BI-building is then modelled as an equivalent elastic SDOF system, whose stiffness is taken equal to the effective stiffness of the IS, evaluated for the design base displacement. Consequently, a uniform acceleration profile over the height of the building is assumed and the equivalent static seismic forces (F_i) are computed by distributing the design base shear (V_b) over the height of the structure, proportionally to the storey masses (m_i):

$$F_i = V_b \frac{m_i}{\sum m_j} \tag{1}$$

This is the approach adopted by the European Seismic Code (CEN 1998), for regular low-rise buildings equipped with IS that can be modelled with an equivalent linear viscous-elastic behaviour (CEN 1998). The same lateral load pattern is provided by the new Italian Seismic code (DMI 2008), in which the applicability of the LSA is limited to BI-buildings not exceeding five storeys.

In the US, Chinese and Taiwanese seismic codes (ICBO 1997; NEHRP 1997; ASCE 2005; ICC 2000; GB50011 2001) a different approach is followed, based on the assumption of an inverted triangular distribution of storey accelerations over the height of the structure, to account for the higher mode contributions generated by possibly nonlinear behaviour of the IS. In this case, the equivalent static seismic forces (F_i) are computed by distributing the design base shear (V_b) over the height of the structure, proportionally to the product of storey masses (m_i) and storey height (h_i):

$$F_i = V_b \frac{m_i \cdot h_i}{\sum m_j \cdot h_j} \tag{2}$$

In the US seismic code, the applicability of the LSA is limited to BI-buildings not exceeding four storeys.

The inverted triangular force distribution defined by Eq. 2 has been found to overestimate the maximum seismic responses of most BI-buildings (Lee et al. 2001), even when the IS exhibits a strong nonlinear behaviour or large effective damping values.

As a mater of fact, the use of LSA is somewhat limited by current seismic codes, due to the difficulty of defining a reasonably conservative distribution of equivalent static seismic forces, as soon as the behaviour of the isolation system is non-linear and/or the damping is high. Nevertheless, the linear static procedure is often performed even when a modal response spectrum analysis is strictly required, to obtain limits on the results of dynamic analysis.

A completely different approach is proposed in the Japanese guidelines for seismically isolated structures (MVIT 2001). Storey shear forces are evaluated from a complex relation-

ship, which depends on the fundamental period of vibration of the BI-structure and on the elastic, viscous and hysteretic components of the design base shear. Storey shear-force distributions intermediate between those given by Eqs. 1 and 2 are thus obtained. The Japanese guidelines do not apply any limitation to the degree of non-linearity of the IS, whereas they refer to accurate force distributions, which depend on the inherent mechanical characteristics of the IS.

Recently, two different groups of researchers (Tsai et al. 2003; Lee et al. 2001) proposed two similar modified equations for the vertical distribution of the equivalent static forces, considering the influence of the first mode of vibration of the BI-structure. The proposed equations can be expressed as follows:

$$F_i = V_b \frac{m_i \cdot \left(1 + \frac{\varepsilon}{H_e} \cdot h_i\right)}{\sum m_j \cdot \left(1 + \frac{\varepsilon}{H_e} \cdot h_j\right)} \tag{3}$$

where $\varepsilon = \omega_b^2/\omega_s^2$, ω_s being the circular frequency of the FB-structure and ω_b that of the BI-structure with the superstructure assumed to behave like a rigid body. H_e represents the effective height of the equivalent SDOF system of the BI-structure, considering the flexibility of the superstructure. The main difference between the equations proposed by Lee et al. (2001) and Tsai et al. (2003) is that, with reference to framed structures, the former assumes $H_e = 0.6H$ whilst the latter assumes $H_e = H$, where H is the total height of the superstructure. In essence, the force distribution given by Eq. 3 corresponds to a trapezoidal distribution of storey acceleration over the height of the structure, which tends to a uniform distribution when $\varepsilon \ll 1$ (i.e. when the superstructure becomes much stiffer than the IS). Similarly to Eqs. 1 and 2, the application of Eq. 3 is limited to low-rise buildings whose IS's can be modelled as equivalent linear viscous-elastic systems.

Some researchers, such as Kelly (2001), Skinner et al. (1993), Constantinou et al. (1993), Winters and Constantinou (1993) performed Nonlinear Time-History Analyses (NTHA) to examine the distribution patterns of lateral inertia forces in BI-buildings with elastic superstructure. They found that the envelope profiles of the storey shear-forces can significantly differ from those derived from Eqs. 1 and 2, even when the BI-structure complies with the requirements for the applicability of LSA. Moreover, they found that the envelope profiles of the storey shear-forces can vary considerably from one case to another, mainly due to the following three factors: (i) the degree of non-linearity of the IS and more precisely the "fatness" of its force-displacement cyclic behaviour, (ii) the number of storeys of the building and (iii) the fundamental period of vibration of the superstructure in the Fixed-Base (FB) configuration.

To quantify the degree of non-linearity of the IS, Skinner et al. (1993) introduced the non-linearity factor NL, defined as the ratio of the area of the hysteresis loops (W_d) at the IS design displacement (D_d) to that of the corresponding rectangle:

$$NL = \frac{W_d}{4 \cdot D_d \cdot F_d} \tag{4}$$

F_d being the IS force at the design displacement D_d. From Eq. 4, it is seen that the non-linearity factor NL is proportional to the equivalent viscous damping ratio ξ (see Eq. 8). The studies by Skinner et al. confirmed the importance of the NL factor with respect to the shear-force distribution in BI-buildings (Skinner et al. 1993).

Efforts have been made to derive enhanced equivalent static force distributions, able to predict accurately the maximum seismic response of a BI-building, even for medium-rise

buildings with strongly non linear IS's. Based on the results of extensive NTHA on multi-storey framed buildings equipped with IS's with an idealised bilinear hysteretic force-displacement behaviour, Andriono and Carr (1991a,b) proposed the following equivalent static force distribution:

$$F_i = V_b \frac{m_i \cdot h_i^p}{\sum m_j \cdot h_j^p} \tag{5}$$

It is similar to Eq. 2, except for the exponent "p". The authors found that p is strongly correlated to the non-linearity factor NL and the fundamental period of vibration of the FB-structure (T_{fb}) (Andriono and Carr 1991b), but they did not provide any analytical or graphical relationship to derive p as a function of these two parameters.

Similar results have been found by Ryan and York (2007), who proposed an inverted triangle distribution with an additional top force:

$$F_i = (V_s - F_t) \frac{m_i \cdot h_i^k}{\sum m_j \cdot h_j^k} \tag{6}$$

in which V_s is the superstructure base shear (derived from the global base shear V_b based on the ratio of the superstructure mass to the total mass of the building) and F_t is an additional static force applied on the top storey of the building. Both the exponent "k" and the additional top force F_t are expressed, through regression analyses, as a function of the IS equivalent viscous damping ratio ξ and of the fundamental period of vibration of the superstructure in the FB configuration (T_{fb}).

Several studies have been recently conducted for the development of seismic design methods based on displacements, able to overcome the limitations of the current design approaches based on forces, which cannot provide appropriate means for implementing concepts of Performance-based Earthquake Engineering (Bertero and Bertero 2002). One of such methods is the Direct Displacement-Based Design (DDBD) method, proposed by Priestley (1993) and further developed by Priestley (2003) and Priestley et al. (2007). The fundamental goal of DDBD is to obtain a structure which will reach a target displacement profile when subjected to earthquakes consistent with a given reference response spectrum.

The DDBD method has been recently specialized to different structural types, including frame buildings (Pettinga and Priestley 2005), wall buildings (Sullivan et al. 2005), continuous deck bridges (Kowalsky 2002) and structures with seismic isolation (Casas and Jara 2006; Cardone and Dolce 2007; Cardone et al. 2006; Pietra et al. 2008).

Basically, the DDBD method consists of four steps (Priestley et al. 2007). In the first step, the target displacement profile of the structure (Δ_i) is assigned. For BI-buildings, this can be carried out by assigning a suitable displaced shape to the superstructure (e.g. an approximate schematization of its first modal shape) and a target value of the IS displacement (D_d) and maximum interstorey drift (θ_d) (Cardone and Dolce 2007). In the second step, the nonlinear MDOF model of the structure is replaced by an equivalent linear SDOF system, characterised by a given equivalent design displacement (Δ_d), equivalent mass (m_{eq}) and equivalent damping ratio (ξ_{eq}). For BI-buildings, the non-linearities of the MDOF model are generally concentrated in the IS, which is preliminarily modelled with an equivalent linear viscous-elastic behaviour, with effective stiffness (k_{is}) and effective damping (ξ_{is}) defined at the target displacement D_d. In the third step, the period of vibration of the equivalent SDOF system (T_e) is obtained from Response Spectrum Analysis (RSA) and then used to derive the equivalent lateral stiffness (K_e) of the SDOF model and, finally, the design base shear ($V_b = K_e \cdot \Delta_d$). In the last step, the design base shear is distributed

along the height of structures in proportion to storey masses m_i and corresponding displacements Δ_i:

$$F_i = V_b \frac{m_i \cdot \Delta_i}{\sum m_j \cdot \Delta_j} \tag{7}$$

A linear static analysis of the structure is then performed, with the IS modeled through its effective stiffness at the design displacement D_d, to get stresses and deformations in the structural members.

Indeed, the lateral force distribution assumed in the DDBD method is very similar to that of the European seismic code (see Eq. 1). As a consequence, the same above discussed shortcomings hold also for the lateral force distribution used within the DDBD method. In particular, significant underestimates are expected as soon as the behaviour of the IS is non linear and/or the damping is high. Actually, multi-storey BI-buildings equipped with IS characterised by thin hysteresis loops are strongly first mode dominated, as the results of a parametric investigation of NTHA on a four-storey three-dimensional framed building equipped with a great variety of IS types confirm (Cardone and Dolce 2007). In this case, the equivalent static forces adopted in the DDBD method provide accurate predictions. On the contrary, when the IS presents relatively large hysteresis loops, the contributions of the higher modes become more significant, especially in the upper storeys, and this causes the storey-shear envelope to be more bulged. In this case, the equivalent static force distribution adopted in the DDBD method turns out to be considerably underestimating.

In this paper, a new approach for the evaluation of accurate lateral force distributions for the LSA of BI-buildings is proposed. The lateral force distributions are specialised to each IS type, accounting for its actual nonlinear mechanical behaviour and isolation ratio T_{is}/T_{fb}. The proposed approach is fully compatible with the Direct Displacement-Based Design (DDBD) method.

2 Isolation systems

Several types of isolation systems are in use today and many new solutions are continuously proposed and investigated (Skinner et al. 1993; Priestley et al. 2007; Higashino and Okamoto 2006; Naeim and Kelly 1999). The most widely used IS's include: (i) Lead-Rubber Bearings (LRB), (ii) High-Damping Rubber Bearings (HDRB), (iii) Friction Pendulum Bearings (FPB) with either single concave configuration (Al-Hussaini et al. 1994) or double concave configuration with equal friction on the two sliding interfaces (Fenz and Constantinou 2006), (iv) Combinations of either Low-Damping Rubber Bearings (LDRB) or FPB with Viscous Dampers (VD), (v) Combinations of flat Sliding Bearings (SB) and LDRB, (vi) Combinations of flat SB and Steel yielding Devices, (vii) Combinations of flat SB, SMA-based re-centring devices (Dolce et al. 2000) and VD. In this study the attention is focused on three groups of IS's, differing in the shape of their hysteresis loops, namely: (a) HDRB and LRB, (b) single concave or double concave FPB and SB + LDRB, (c) SB + SMA. The results of this paper do not apply to the spherical sliding IS's with adaptive behaviour, recently proposed by Fenz and Constantinou (2007a,b).

The cyclic hysteretic behaviour of HDRB and LRB can be described by an Elasto-Plastic with Hardening (EPH) force-displacement model, that of FPB and SB+LDRB by a Rigid-Plastic with Hardening (RPH) model, finally, that of SB + SMA by a Flag-Shaped (FS) model. Actually, in accordance with (Naeim and Kelly 1999; Ryan and Chopra 2004; Scheller and Constantinou 1999), the cyclic behaviour of FPB and SB + LDRB can also be described by

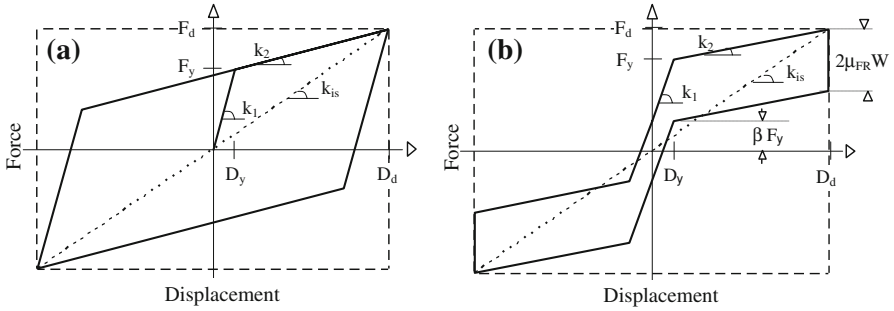

Fig. 1 Schematic force-displacement behaviour of IS's responding according to an (**a**) Elasto-Plastic with Hardening (EPH) and (**b**) Flag-Shaped (FS) model

an EPH relation, requiring only the specification of a different value for the yield displacement. In particular, the yield displacement for FPB and SB + LDRB can be assumed lower than 5 mm while that of LRB and HDRB is greater than 5–10 mm. For simplicity, in the remaining of the paper, reference will be carried out to RPH and EPH models to distinguish EPH models with yield displacement lower than 5 mm and greater than 5 mm, respectively.

Figure 1 shows the idealised force-displacement behaviour of IS's responding according to EPH (Fig. 1a) and FS (Fig. 1b) models. The numerical parameters that identify each model are also reported in Fig. 1. The models present a stiffness k_1 before yielding/sliding ($D < D_y$) and a lower stiffness k_2 during yielding/sliding ($D > D_y$). The ratios $\alpha = k_2/k_1$ and $\mu = D_d/D_y$ are the post-yield hardening and ductility ratio of the IS, respectively.

By analogy with the linear systems, the stiffness k_1 and k_2 can be related to corresponding periods of vibration of the BI-structure, named T_1 and T_2 respectively. The yield ratio F_y/W relates the yield force of the IS to the weight of the structure. Based on the criterion of minimizing both top floor accelerations and IS displacements, the optimum values of F_y/W are found to be in the range of 5–10% under far-fault earthquakes (Skinner et al. 1993; Jangid 2007).

As stated before, in the DDBD method the IS's are modelled through their effective stiffness k_{is} and effective damping ratio ξ_{is}. The effective stiffness is defined as the secant stiffness to the design displacement D_d (see Fig. 1). The effective stiffness is related to the effective period of the IS. The effective damping ratio is proportional to the ratio of the area enclosed by the hysteresis loops W_d to the strain energy W_s at the maximum displacement amplitude (Chopra 1997):

$$\xi_{is} = \frac{1}{4\pi} \cdot \frac{W_d}{W_s} = \frac{W_d}{2\pi \cdot F_d \cdot D_d} \tag{8}$$

It is then apparent that a direct proportionality between the effective damping ξ_{is} and the non-linearity factor NL exists (compare Eqs. 4 and 8). The non-linearity factor increases from 0 to 1 as the hysteresis loops change from a zero-area to a rectangular shape. Correspondently, the effective damping ratio increases from 0% to 63%. For the FS systems, another parameter has to be specified. It is the strength ratio β, defined as the ratio of the unloading to loading force at the yield displacement (see Fig. 1b). The parameter β affects the re-centring and energy dissipating capability of the IS. It ranges from 1 (for SMA only) to -1 (for SB only). Both the effective damping ξ_{is} and the non-linearity factor NL of Flag-Shaped IS strongly depend on the strength ratio β.

The higher-mode acceleration response of BI-buildings is mainly determined by the degree of non-linearity of the IS (Skinner et al. 1993). The latter can be estimated by either the

non-linearity factor NL or the effective damping ratio ξ_{is} of the IS. For a given non-linearity factor, however, there are other IS parameters that may affect the higher-mode acceleration response of BI-buildings. They are the period ratios (i) T_1/T_{fb} (ii) T_2/T_1 and (iii) T_{is}/T_{fb}. The period ratio T_1/T_{fb} takes into account the initial elastic stiffness (k_1) of the IS. The period ratio T_2/T_1 is related to the IS post-yield hardening ratio ($\alpha = k_2/k_1$). Each transition of the IS through its elastic phase determines a transfer of energy from the first-mode to the higher-modes. The isolation ratio T_{is}/T_{fb} mainly dominates the first-mode response of the BI-buildings, hence its maximum base displacement and base shear. However, it also affects the degree of coupling and level of excitation of the higher modes. As illustrated in Skinner et al. (1993), the contributions of the higher-modes to the seismic response of BI-buildings equipped with bilinear IS reduce when increasing the period ratios T_1/T_{fb} and T_{is}/T_{fb}, as well as when reducing the period ratio T_2/T_1. Enhanced lateral force distributions for the LSA of BI-buildings are then expected to depend on the aforesaid IS parameters (i.e. NL, T_1/T_{fb}, T_2/T_1 and T_{is}/T_{fb}). Actually, only three of them are needed to univocally identify a given BI-building, once a target value of the IS displacement has been assumed (Step 1 of the DDBD method) and the associated design base shear has been derived from RSA (Step 3 of the DDBD method). The four IS parameters, indeed, are mutually related through Eq. 4.

In order to customize the new equivalent static force distributions to each IS type, typical values of the engineering properties of each IS type have been searched for. The typical values reported below have been collected from different sources, including: literature review, data from manufacturers, code requirements and common applications. Obviously, the attention has been focused on the IS mechanical properties mainly related to the DDBD concepts, such as those defining the displacement capacity and equivalent viscous damping capacity of the IS. More detailed information on this topic can be found in Skinner et al. (1993), Naeim and Kelly (1999), Priestley et al. (2007), Kelly (2001), HITEC (1998) and in the data sheets and product brochures of Bridgestone Inc., DIS Inc., Skellerup Ind., TIS S.p.A., FIP S.p.A., ALGA S.p.A.

Figure 2 shows how the phenomenological force-displacement relationship of the three types of IS's considered in this study, i.e.: (a) HDRB/LRB, (b) FPB/SB+LDRB and (iii) SB + SMA can be modeled as a suitable combination of simpler model components.

The cyclic behaviour of LRB/HDRB (see Fig. 2a) is captured by combining in parallel an Elasto-Perfectly Plastic element, modeling the confined lead core of LRB or the hysteretic energy dissipation capacity of HDRB, with a Linear Viscous-Elastic element, modeling the shear stiffness and viscous damping of rubber.

The lead plug exhibits an initial shear modulus approximately equal to 130 MPa, while that of rubber at 100% shear strain typically ranges from 0.5 to 1.2 MPa, and a yield shear strain of approximately 7.7% (Skinner et al. 1993; Kelly 1992). The yield displacement of LRB is, therefore, approximately equal to 7.7% H, H being the height of the device. Typical heights of LRB vary from 100 to 350 mm (Skellerup Ind.; DIS Inc.; Bridgestone Inc.) and then, yield displacements ranging from 7.7 to 26.7 mm are expected. In the common practice, the cross section area of the lead plug is equal to 5–10% the gross section area of rubber (Robinson 1982; Skinner et al. 1993), so that post-yield hardening ratios of the order of 5–15% are expected (Kelly 2001; Priestley et al. 2007). The maximum displacement capacity of LRB is governed by the allowable shear strain in the rubber and by the global stability of the device under vertical load. Hence, it is governed by the total height of rubber and the cross section dimensions of the device (diameter D for circular bearings, side dimensions b_x and b_y for rectangular bearings). Typically, design displacements between 120 and 350 mm, corresponding to rubber shear strains of 100–120% and ductility ratios of the order of 10–20, are assumed for LRB, although much greater rubber shear strains (200–250%) and ductility

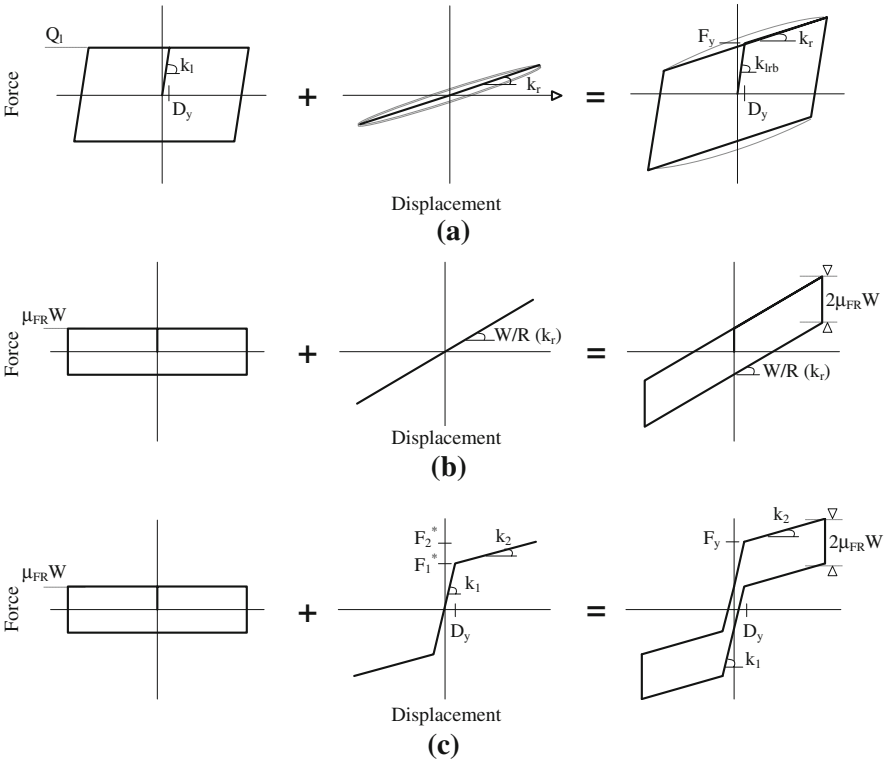

Fig. 2 Combination of basic IS components for the modeling of the mechanical behaviour of (**a**) LRB/HDRB, (**b**) FPB/SB + LDRB and (**c**) SB + SMA isolation systems

Table 1 Typical effective damping ratios (ξ_{is}) and non-linearity factors (NL) of different IS types

IS type	Numerical model	ξ_{is} (%)	NL
HDRB	EPH	15–20	0.25–0.30
LRB		20–30	0.30–0.47
$(FPB)_{lub}$	RPH	10–25	0.16–0.40
$(FPB)_{pure}$		25–32	0.40–0.50
SB + LDRB		15–30	0.25–0.47
SB + SMA	FS	6–30	0.10–0.47

ratios (20–40) can be cyclically sustained (Skinner et al. 1993). The aforesaid limits lead to effective damping ratios ranging from 20% to 30%, corresponding to non-linearity factors approximately between 0.3 and 0.5 (see Table 1). For the sake of clarity, it is worth to emphasize once again that the values of effective damping and non-linearity factor reported in Table 1 refer to the typical design displacements of each IS type. As known, the effective damping (hence the NL factor) strongly depends on the ductility ratio. Values of the NL factor out of the ranges listed in Table 1 may be expected for ductility ratios lower or greater than the design limits, e.g. as a consequence of PGA's lower or greater than the design value.

The idealised cyclic behaviour of HDRB is substantially similar to that of LRB, except for the initial elastic stiffness k_1 (see Fig. 1), which turns out to be significantly lower than

LRB. Equivalent yield displacements greater than 25 mm and post-"yield" hardening ratios between 15% and 25% are expected (Naeim and Kelly 1999). Effective damping ratios of the order of 15–20% and corresponding non-linearity factors of the order 0.25–0.3 are typically found (see Table 1). Actually, LRB and HDRB with diameter as large as 1500 mm and isolator height up to 500–650 mm are commercially available (e.g. see DIS-Inc brochure). For these latter the (nominal) displacement capacity attains 900 mm.

The cyclic behaviour of FPB/SB+LDRB (see Fig. 2b) is captured by combining, in parallel, a Rigid-Perfectly Plastic element, modeling the frictional behaviour of flat or curved SB, with a Linear Viscous-Elastic element, modeling the geometry-based re-centring mechanism of FPB or the shear stiffness and viscous damping of LDRB. Sliding Bearings used in seismic isolation typically exploit the low friction between PTFE (Polytetrafluoroethylene or Teflon) pads in contact with lubricated polished stainless steel surfaces (Constantinou et al. 1990). The dynamic friction coefficient of PTFE-steel Sliding Bearings depends on a number of factors, the sliding surface conditions, the bearing pressure, the velocity of movement and the air temperature being the most important ones (Mokha et al. 1990). The friction coefficient of lubricated PTFE-steel Sliding Bearings normally vary between 2% and 5%, while increasing up to 10–12% for pure PTFE-steel surface (Dolce et al. 2005). As known (Al-Hussaini et al. 1994), the post-sliding stiffness of single concave FPB is defined as W/R_c, where R_c is the effective radius of curvature of the sliding interface and W the supported weight. Similarly, for double concave FPB with equal friction on the two sliding interfaces (Fenz and Constantinou 2006), the post-sliding stiffness is defined as $W/(R_{c1}+R_{c2})$, R_{c1} and R_{c2} being the radii of curvature of the two sliding surfaces. In principle, there is no theoretical limit to the displacement capacity of FPB, provided that a device with the required dimensions can be manufactured. Actually, the horizontal displacement capacity of FPB is conditioned by the acceptability of the corresponding vertical displacement and residual horizontal displacement. Both are a function of the radius of curvature R_c. As a consequence, limitations to the ratio between the design IS displacement D_d and the radius of curvature R_c are necessary to limit vertical and residual displacements. Reasonable values of the ratio D_d/R_c are between $\mu_{FR,\,max}$ (e.g. 5% for lubricated interfaces) (Naeim and Kelly 1999) and 15% (Priestley et al. 2007). FPB with radius of curvature, ranging from 1 to 10 m, are commercially available (Naeim and Kelly 1999). Considering the aforesaid parameters, effective damping ratios of the order of 10–25% and non-linearity factors approximately between 0.16 and 0.4 are found for FPB with lubricated surfaces (see Table 1). The idealised cyclic behaviour of SB + LDRB is substantially very similar to that of LRB, except for the re-centring capacity of the systems, which relies upon the shear stiffness of rubber (k_r). The viscous damping of rubber ($\approx$5%) leads to greater effective damping ratios (hence higher non-linearity factors) compared to FPB (see Table 1).

As an alternative to LDRB, the SMA-based re-centring devices, recently designed, implemented and tested (Dolce et al. 2000), can be used. The main advantage of SMA-based re-centring devices, compared to rubber-based re-centring devices, is the best control of the force transmitted to the superstructure (Dolce et al. 2007). The SMA-based devices proposed by Dolce et al. (2000) exhibit a cyclic behaviour which can be schematized as bilinear elastic, although some energy is also dissipated by SMA, typically resulting in 3–5% damping. An IS characterised by double Flag-Shaped (FS) hysteresis loops (see Fig. 1c) is obtained by combining, in parallel, the SMA-based re-centring device with lubricated flat SB (Dolce et al. 2007).

Based on the experimental results of cyclic tests on SMA devices (Dolce et al. 2000), the following practical values of the design parameters of the SMA device can be assumed: yield displacement lower than 10 mm and post-yield hardening ratio ranging from 1% to 5%. The

energy dissipation and re-centring capacity of SB + SMA is governed by the strength ratio β, defined as (see Fig. 2b):

$$\beta = \frac{F_1^* - \mu_{FR} \cdot W}{F_1^* + \mu_{FR} \cdot W} \tag{9}$$

The strength ratio β should be maintained greater than about 0.25, in order to guarantee a full re-centring behaviour of the IS (Cardone et al. 2006). Based on the selected parameters, the effective damping ratios of SB + SMA can vary between 6% and 30% and the corresponding non-linearity factors between 0.1 and 0.47 (see Table 1). In principle, there is no theoretical limit to the displacement capacity of IS's based on pre-strained SMA wires. In practice, it is strongly conditioned by the maximum device dimensions that can be accepted. It seems reasonable to consider design displacements not greater than 350 mm.

3 Formulation of the 3-MM force distribution

The distributions of the maximum storey shear-forces experienced by BI-buildings with non-linear IS (see Sect. 5.) are strongly different from the uniform (first-mode) distribution and show a marked bulge at the mid-height of the building, due to the higher-mode acceleration response discussed before (see Sect. 2.).

The proposed lateral force distributions present a formulation which is formally given by Eq. 7, where the "displacement" profile Δ_i is now expressed as a linear combination of the first three approximate modal shapes of the BI-building with the IS modelled through its effective stiffness at the design displacement D_d. For this reason, the acronym 3-MM (3-Mode Method) can be used to identify the proposed approach. It should be observed that the "displacement" profile of Eq. 7 actually represent the distribution of maximum storey accelerations generated by the earthquake over the height of the building. Modal acceleration profiles, indeed, have the same shape as the corresponding displacement profiles but are of opposite sign. Therefore, the actual improvements of the proposed approach mostly consist in an accurate evaluation of the higher-mode acceleration response of the BI-building.

The step-by-step procedure followed in this study to derive the 'enhanced' lateral force distributions is described in Fig. 3 and summarised below.

- Step 1: NTHA of prototype BI-buildings equipped with a great variety of IS's, using a set of seven spectrum-compatible accelerograms;
- Step 2: Average (over seven accelerograms) of the maximum storey shear-forces and maximum IS displacements obtained from NTHA. Normalization of the storey shear-force distributions, assuming $V_b = 1$;
- Step 3: Evaluation of the isolation ratio T_{is}/T_{fb}, based on the maximum IS displacement obtained in step 2, modelling the BI-buildings as SDOF systems;
- Step 4: Evaluation of approximate modal shapes for the first three modes of vibration of the BI-building. In accordance with (Skinner et al. 1993), they can be expressed as follows:

$$\phi_{1i} = \cos\left[\left(\frac{T_{is}}{T_{fb}}\right)^{-1} \cdot \left(1 - \frac{i}{N}\right) \cdot \frac{\pi}{2}\right] \tag{10}$$

$$\phi_{ji} = \cos\left[(2N-2) \cdot \frac{\pi}{2} \cdot \frac{i}{N}\right] \quad \text{for} \quad j \geq 2 \tag{11}$$

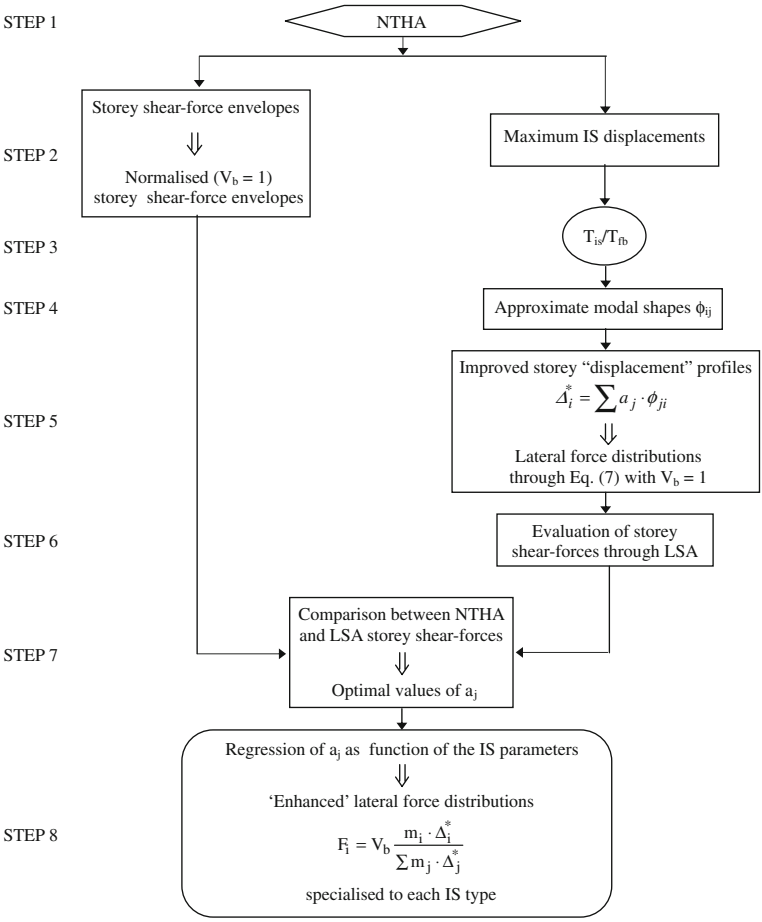

Fig. 3 Step-by-step procedure followed in this study to derive 'enhanced' lateral force distributions for the LSA of BI-buildings

where N is the number of storeys of the BI-building and T_{is}/T_{fb} its isolation ratio. Eqs. 10 and 11 correspond to the exact modal shapes of a continuous shear building. Frame buildings with equal-mass rigid floors and uniform storey-stiffness can be approximated as a continuous shear building;

– Step 5: Derivation of improved "displacement" profiles and evaluation of the associated lateral force distributions through Eq. 7, assuming $V_b = 1$. The new "displacement" profiles are obtained as linear combinations of the approximate first three modal shapes derived in step 4 (see Fig. 4):

$$\Delta_i^* = \phi_{1i} + a_2 \cdot \phi_{2i} + a_3 \cdot \phi_{3i} \tag{12}$$

where ϕ_{1i}, ϕ_{2i} and ϕ_{3i} are the approximate shapes of the first, second and third mode of vibration, respectively;

– Step 6: LSA of the prototype BI-buildings, using the lateral force distributions obtained in step 5;

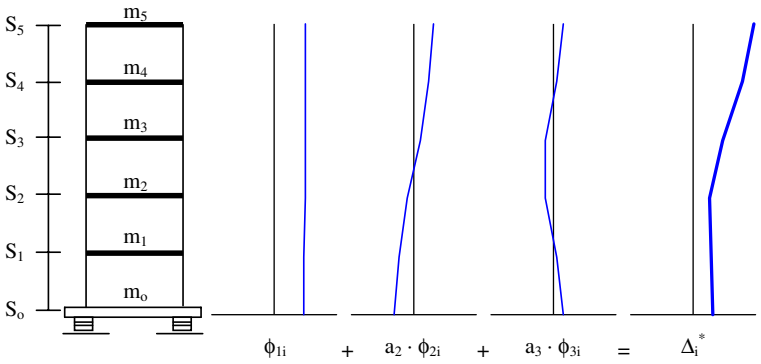

Fig. 4 Acceleration profiles for the evaluation of enhanced lateral force distributions

– Step 7: Comparison between NTHA and LSA storey shear-forces and evaluation of the optimal values of the coefficients a_2 and a_3 based on the least squares method;
– Step 8: Multivariate regression analysis of the optimal values of a_2 and a_3 obtained in step 7, as a function of a number of selected IS parameters (NL, T_1/T_{fb} and T_{is}/T_{fb}), related to its nonlinear cyclic behaviour.

At the end of the step-by-step procedure described below, a final check of the general accurateness of the proposed 3-M method has been executed, comparing the storey shear-forces derived from NTHA with those obtained from LSA, using both standard and the enhanced force distributions.

4 Numerical models

The main aim of the NTHA was to evaluate the envelopes of the maximum storey shear-forces associated to the seismic response of prototype buildings of different heights, equipped with different types of IS. Distributions of equivalent-static-forces compatible with the shear profiles provided by NTHA have been then derived. NTHA have been carried out by using the structural analysis program SAP2000 (2004). The modelling assumptions are described in detail in the next sections, separately for superstructure, IS and seismic ground motion.

4.1 Seismic ground motion

A set of seven natural and artificial ground acceleration-time histories (see Fig. 5a), compatible (on average) with a modified version of the displacement response spectrum provided by Eurocode 8 (CEN 1998) for soil type C, has been used in the numerical simulation analyses. Actually, the only difference with respect to the standard EC8-soil C spectrum consists in the corner period T_D, corresponding to the transition from the constant-velocity to the constant-displacement region of the spectrum, which has been taken equal to 4 s instead of 2.5 s. This assumption is justified by the results of recent studies by Faccioli et al. (2004), which show that the corner period T_D increase almost linearly with earthquake magnitude. Based on the examination of the shape of displacement spectra derived from a great number of recent high-quality digital records, Faccioli and co-workers proposed the following relationship for the evaluation of the corner period T_D:

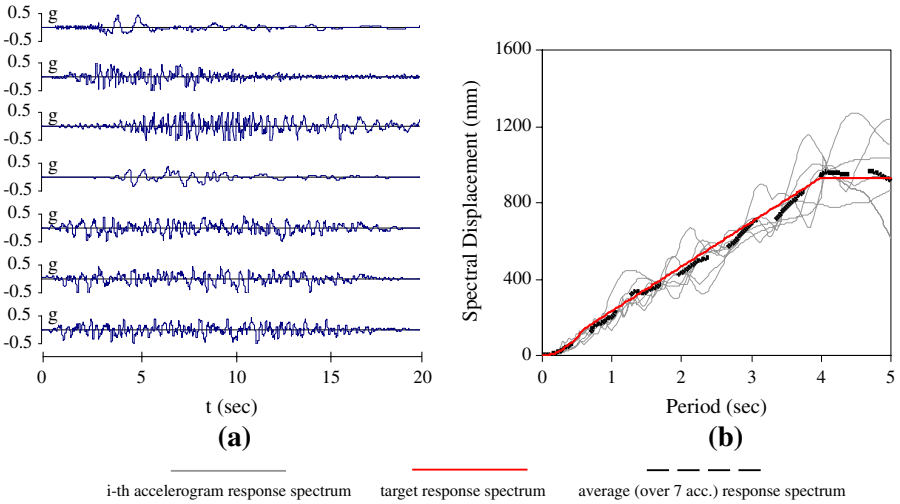

Fig. 5 (**a**) Set of ground acceleration-time histories adopted in NTHA. (**b**) Comparison between the 5%-damped target response spectrum and the average response spectrum of the selected earthquake ground motions. PGA = 0.5 g

$$T_D = 1.0 + 2.5 \cdot (M_w - 5.7) \tag{13}$$

where M_w is the moment magnitude of the earthquake. According to Eq. 13, a corner period of 4 s, as that assumed in this study, corresponds to a moment magnitude $M_w = 6.9$.

In Fig. 5b the target response spectrum adopted in this study is compared to the average response spectrum associated to the selected earthquake ground motions. In the NTHA, the peak ground acceleration (PGA) has been progressively increased from 0.1 to 1 g (step 0.1 g), in order to cover the range of isolation ratios T_{is}/T_{fb} reported in Table 2. In the evaluation of the effective period of the BI-structure (T_{is}), reference has been carried out to an equivalent elastic SDOF system with effective stiffness equal to the secant stiffness at the mean value (average over 7 accelerograms) of the maximum IS displacement.

In the NTHA, each BI-building configuration was analyzed for a 20 s duration of each accelerogram, at a time step of 0.01 s. At each time step, shear-forces and displacements at each level of the BI-structure have been saved and then processed as described in the next sections.

4.2 Superstructure

Six different prototypes of multi-storeys shear-type frame buildings, differing in the number of storeys (3, 5 or 8, precisely) and fundamental period of vibration in the fixed-base configuration, have been considered for the NTHA. The buildings have been modelled as MDOF systems with lumped masses. They have been assumed to have same floor mass and same storey stiffness at all the levels, including the base floor (see Fig. 6). Each floor mass (m) has been computed referring to residential buildings with gross floor area of 200 m^2, resulting equal to 14 ton. For each prototype building, the storey stiffness (k) has been adjusted to provide two different target fixed-base fundamental periods of vibration. These latter have been derived based on two well-known approximate relationships (CEN 1998):

$$T_{fb} = C \cdot H^{3/4} \tag{14}$$

Table 2 IS parameters and period ratios considered in the NTHA

IS type	F_y/W	β	T_1 (s)	D_y (mm)	α (%)	T_2/T_1	T_1/T_{fb}	T_{is} (s)	T_{is}/T_{fb}	D_{max} (mm)
LRB/HDRB	0.05 0.10	–	0.60 0.90 1.20	>5 ≤ 35 (6 var.)	5.0 10.0 15.0 20.0	4.47 3.16 2.58 2.24	0.75–4.8 (18 var.)	0.8–6.0 (1440 var.)	1–20 (1440 var.)	35–800 (1440 var.)
FPB/SB + LDRB	0.05 0.10	–	0.15 0.30	≤ 5 (4 var.)	0.1 0.5 1.0 3.0	31.63 14.24 10.00 5.77	0.19–1.2 (12 var.)	0.6–7.0 (960 var.)	0.8–30 (960 var.)	20–1000 (960 var.)
SB + SMA	0.03–0.13 (48 variations)	−0.66 −0.30 −0.15 0.00 0.15 0.30 0.45 0.66	0.40 (N = 3) 0.50 (N = 5) 0.60 (N = 8)	0.44–5.93 (48 var.)	1.0 3.0	10.00 5.77	0.76–1.64 (6 var.)	1.2–3.0 (960 var.)	2.50–4.0 (960 var.)	80–300 (960 var.)

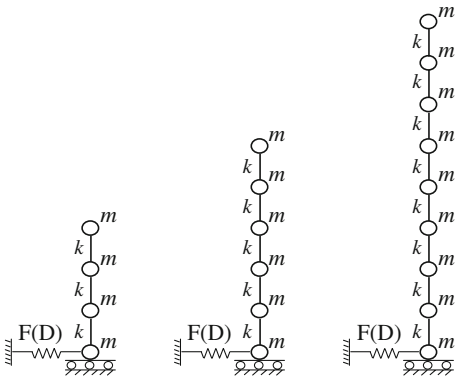

Fig. 6 Layout of the prototype BI-buildings examined in this study

and

$$T_{fb} = N/12 \tag{14'}$$

where C = 0.075 for RC buildings, H is the total height (in meters) of the building and N is the number of storeys. Assuming a constant interstorey height of approximately 3.1 m, the following variations of fundamental period have been considered: (i) $T_{fb} = 0.25 - 0.4$ s for the 3-storey building, (ii) $T_{fb} = 0.4 - 0.6$ s for the 5-storey building and (iii) $T_{fb} = 0.65 - 0.8$ s for the 8-storey building. 5% damping ratio has been considered for the superstructure.

4.3 Isolation systems

The IS has been modelled with a nonlinear spring element placed at the base floor of the building (see Fig. 6). As stated before, two different force-displacement models (see Fig. 1) have been used to the describe the cyclic behaviour of a great variety of IS types (see Fig. 2 and Table 1).

A total of 24 LRB/HDRB (2 yield ratios × 3 elastic periods × 4 post-yield hardening ratios), 16 FPB/SB + LDRB (2 yield ratios × 2 elastic periods × 4 post-yield hardening ratios) and 16 SB + SMA (8 strength ratios × 2 post-yield hardening ratios) isolation systems have been considered in the NTHA.

It is worth to remember that the elastic and post-elastic stiffness of the IS (k_1 and k_2, respectively) are related to the elastic and post-elastic period of the BI-building (T_1 and T_2, respectively) through the following relationship:

$$k_i = 4\pi^2 \cdot \frac{N \cdot m}{T_i^2} \tag{15}$$

where N is the total number of storeys of the building, including the base floor.

Approximately, some 25000 NTHA (56 IS configurations × 6 prototype buildings × 10 PGA levels × 7 accelerograms) have been performed. For each BI-building configuration, reference to the average seismic response, derived from the selected (7) accelerograms, has been then carried out. Since the overall behaviour parameters, such as the non-linearity factor NL, the effective period of vibration T_{is}, the ductility ratio μ and the maximum displacement capacity D_u, depend on the amplitude of the response, the average NTHA results have been then filtered in order to select only the cases which comply with suitable ranges

of these parameters ($0.15 < NL < 0.65$, $T_{is}/T_{fb} \geq 2.0$, $T_{is} \leq 4\,s$, $\mu < 40$, for LRB/HDRB only, and $D_u < 350\,mm$, for SB + SMA only).

Indeed, approximately 1500 average storey shear-force distributions have been selected and then used to derive the 3-MM lateral force distributions presented in the next sections. It should be noted that the range of NL factors taken into account is slightly wider than those typically associated to the IS types under examination (see Table 1). This has been purposely done, in order to extend the applicability of the proposed formulation. The two limit values of NL selected (i.e. NL = 0.15 and NL = 0.65) have a precise physical significance, as shown in Sect. 6.

5 Non linear analysis results

Figure 7 shows some typical envelopes of maximum storey shear-forces obtained from NTHA. They are normalized with respect to the maximum base shear, so that $V_b = 1$ for all of them. The diagrams of Fig. 7 refer to the 5-storey building with $T_{fb} = 0.6\,s$, equipped with different bilinear hysteretic IS's with the same yield ratio ($F_y/W = 0.05$). They are compared to the shear-forces derived from LSA using uniform and inverted triangular lateral force distributions.

Figure 7 clearly shows that there are three major factors that influence the shape of the storey shear envelopes: (i) the post-yield hardening ratio α, (ii) the period ratio T_1/T_{fb}, related to the initial stiffness (k_1) of the IS and (iii) the isolation ratio T_{is}/T_{fb}, related to the effective stiffness (k_{is}) of the IS. Changes in the aforesaid parameters yield to variations in the shape and 'fatness' of the IS hysteresis loops, well pointed out by the different values of the non-linearity factor NL associated to each shear envelope. Figure 7a, in particular, shows the effect of varying the post-yield hardening ratio while keeping the initial stiffness ($T_1/T_{fb} = 1$), the yield displacement ($D_y = 8.95\,mm$) and the ductility ratio ($\mu \cong 20$) unchanged. As can be observed, the non-linearity factor NL strongly increases as the post-yield hardening ratio reduces. As a consequence, the shear envelope becomes more and more nonlinear. Figure 7b shows the effect of varying the period ratio $T_1/T_{fb} = 1$ while keeping the post-yield hardening ratio ($\alpha = 5\%$), the ductility ratio ($\mu \cong 20$) and, more importantly, the non-linearity

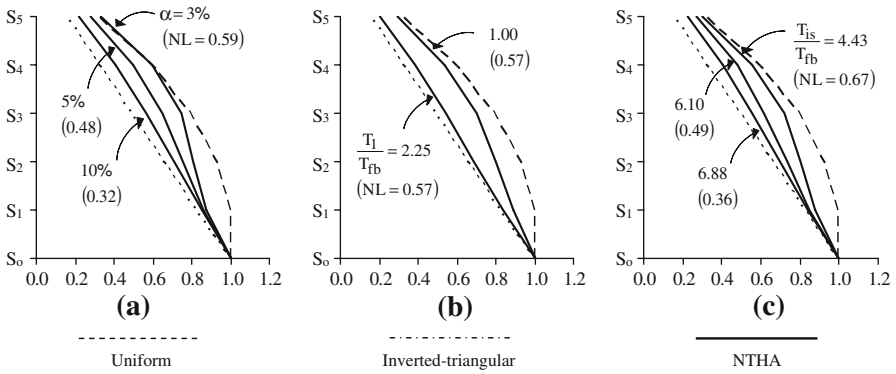

Fig. 7 Five-storey prototype building equipped with different bilinear IS's ($F_y/W = 0.05$) characterised by (**a**) $T_1/T_{fb} = 1$ and $\mu \cong 20$, (**b**) $\alpha = 5\%$ and $\mu \cong 12$ and (**c**) $\alpha = 5\%$ and $T_1/T_{fb} = 1.5$. Comparison between shear-forces obtained from NTHA and LSA using uniform and inverted triangular lateral force distributions

factor (NL = 0.57) unchanged. As can be observed, the shear envelope tends to a linear profile while increasing the period ratio T_1/T_{fb}. A similar result is also found as the isolation ratio T_{is}/T_{fb} increases (see 7c).

There is an apparent correlation between the NL factor and the shape of the shear envelope: as the NL factor increases, the shear envelope becomes more bulged, indicating more significant higher-mode contributions. However, two further parameters (e.g. T_1/T_{fb} and T_{is}/T_{fb}), appraising the higher-mode contribution to the seismic response of the BI-building, must be accounted for.

Another interesting observation from Fig. 7 is that both the uniform and the inverted triangular equivalent-static-force distribution are inadequate to describe the great variety of situations that can be found. Indeed, the uniform distribution (as well as the force distribution used in the standard DDBD method) leads to significant underestimates in the prediction of the maximum seismic stresses, even for relatively low NL factors (say of the order of 0.25–0.3), especially at the upper storeys of the building. On the other hand, the inverted triangular distribution results too conservative in many cases. For relatively high NL factor (say of the order of 0.5–0.6), the inverted triangular distribution provides reasonably accurate results at the upper storyes while it largely overestimates the maximum seismic stresses at the lower storeys. Similar considerations hold for the SB + SMA isolation systems, though they take place for reduced values of the NL factor.

The aforesaid limitations in the use of the LSA for BI-buildings can play a fundamental role in the accuracy of the DDBD predictions, since the DDBD method expressly relies upon LSA for the evaluation of the maximum stresses in the structural members. However, the aforesaid limitations may have important implications also for the force-based design approaches on which current seismic codes (CEN 1998; ICBO 1997; NEHRP 1997) are based, as many IS and building configurations examined in this study (e.g. most of the 3- and 5-storey buildings with LRB/HDRB isolation systems) comply with the general requirements for the applicability of LSA. It is clear that accurate predictions from LSA can be achieved only by customising the lateral force distributions to the IS characteristics. This may also give the possibility to extend the applicability of the LSA to a greater number of situations.

6 Proposed lateral force distributions

As stated before (see Sect. 3.), in the proposed formulation, the "displacement" profile Δ_i is expressed as a linear combination of approximate modal shapes of the BI-building (see Eqs. 16–18). For completeness, three different "displacement" profiles have been preliminarily considered:

$$\Delta_{1i}^{*} = \phi_{1i} \tag{16}$$

$$\Delta_{2i}^{*} = \phi_{1i} + a_2 \cdot \phi_{2i} \tag{17}$$

$$\Delta_{3i}^{*} = \phi_{1i} + a_2 \cdot \phi_{2i} + a_3 \cdot \phi_{3i} \tag{18}$$

In the previous equations, ϕ_{1i}, ϕ_{2i} and ϕ_{3i} represent the approximate shapes of the first, second and third mode of vibration of the BI-building, a_2 and a_3 are two coefficients depending on the IS properties and the BI-building characteristics. It should be noted that the displacement profile provided by Eq. 16 is practically the same as that adopted in the standard DDBD method (Priestley et al. 2007; Cardone and Dolce 2007).

Inserting the displacement profiles defined before in Eq. 7 with $V_b = 1$, three alternative lateral force distributions have been drawn for each BI-building configuration examined in this study. Consequently, three different storey shear profiles have been derived from LSA and then compared to those obtained from NTHA, in order to calibrate the coefficients a_2 and a_3. The optimization of the coefficients a_2 and a_3 has been carried out by minimising the differences between LSA and NTHA storey shear-forces with the least square method. The optimization has been conducted separately for each BI-building configuration, considering at the same time all the levels of the structure, with the exception of the IS level ($V_b = 1$ for both LSA and NTHA shear profiles).

As an example, in Fig. 8 some typical shear envelopes obtained from NTHA are compared to those derived from LSA using the optimised lateral force distributions presented before. The comparison is carried out for 3-, 5- and 8-storey buildings ($T_{fb} = 0.4$, 0.6 and 0.8 s, respectively) equipped with different types of IS (LRB, FPB and SB + SMA, respectively) characterized by relatively high NL factors. For completeness, in the diagrams of Fig. 8 the storey shear profiles associated to the uniform and inverted lateral force distributions (see Eqs. 1 and 2) are also reported.

As can be observed, when a displacement profile equal to the first modal shape (1-MM) of the BI-building is assumed (like in the standard DDBD method), a shear profile very similar to that associated to the uniform lateral force distribution is obtained. Therefore, significant underestimates in the LSA predictions are observed, due to the non-linear behaviour of the IS. The discrepancies between LSA predictions and NTHA results increase while increasing the number of storeys. Considering first and second modal shape (2-MM) according to Eq. 17, a conservative estimation of the shear envelopes obtained from NTHA is achieved. The accuracy decreases passing from the upper to the lower storeys of the building. Finally, when also the third mode is taken into account (3-MM) according to Eq. 18, an excellent accordance is observed, throughout the height of the structure.

In order to make the proposed approach really attractive for practical purposes, the coefficients a_2 and a_3 must be expressed as a function of a number of parameters easy to define, through user-friendly analytical or graphical tools.

6.1 Isolation systems with bilinear hysteretic cyclic behaviour

Figure 9 shows the trend of the coefficient a_2 as a function of NL, for different period ratios T_1/T_{fb}, and the correlation between a_2 and a_3. Figure 9 refers to (almost) the totality of NTHA carried out on BI-buildings with bilinear hysteretic IS's (model EPH of Fig. 1). Only the filters relevant to the isolation ratio T_{is}/T_{fb} ($\geq$2.0) and the effective period T_{is} ($\leq$4 s) are applied. In the diagrams, the range where LRB/HDRB and FPB/SB + LDRB typically fall is highlighted. As expected, a_2 increases more than linearly while increasing NL. For a given NL value, a_2 reduces as T_1/T_{fb} increases. a_2 rapidly tends to zero as soon as NL becomes lower than a given limit value, which increases with T_1/T_{fb}. Based on the results of this study, the coefficient a_2 (as well as a_3) can be assumed equal to zero for NL < 0.15. This occurs regardless the value of T_1/T_{fb} and the number of storeys of the building. For NL < 0.15, therefore, reference can be carried out to the first modal shape only (see Eq. 16), as in the standard DDBD method.

The main difference between buildings of different height (compare Fig. 9a–c) consists in the corresponding values of T_1/T_{fb}, which reduce as the height of the building (hence its fundamental period of vibration T_{fb}) increases. As a consequence, the range of NL where only one mode can be considered reliable and accurate narrows.

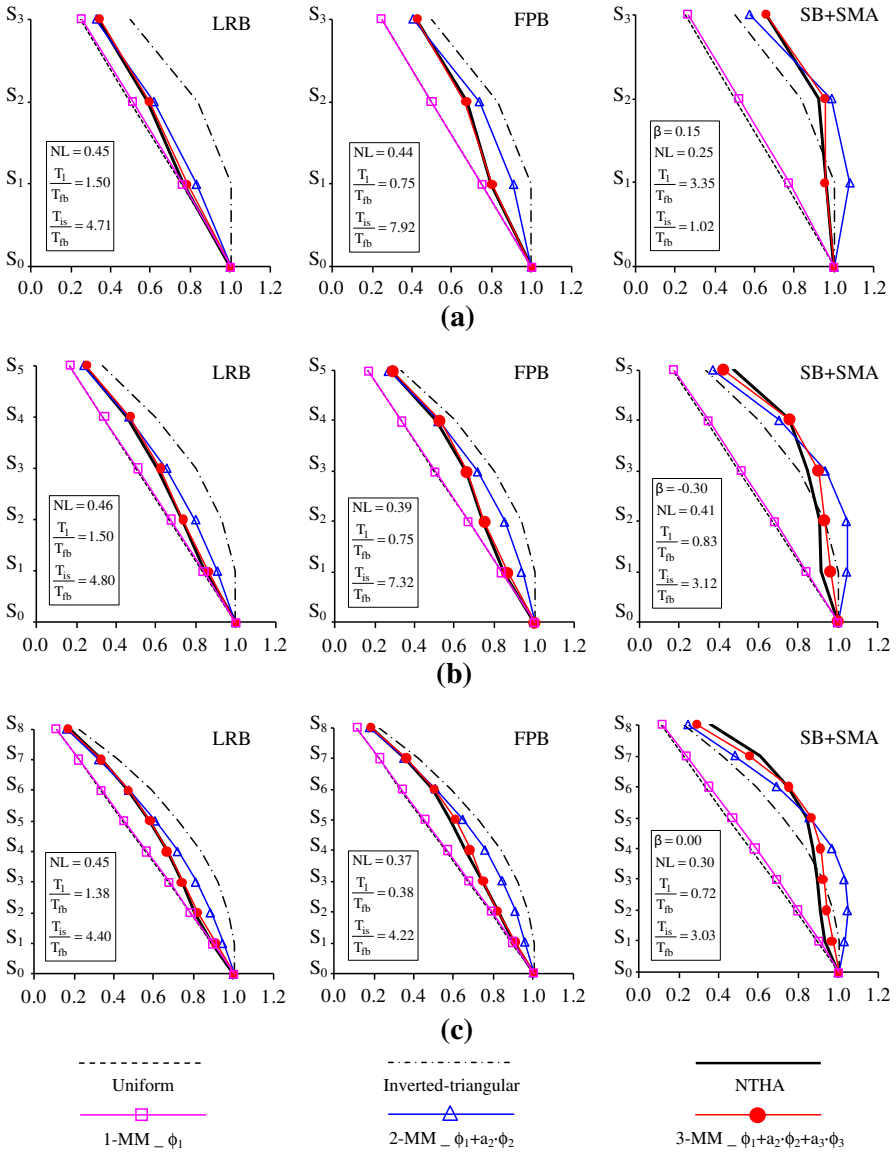

Fig. 8 Comparison between normalized ($V_b = 1$) shear envelopes obtained from NTHA and normalized shear profiles derived from LSA using different lateral force distributions, for (**a**) 3-storey, (**b**) 5-storey and (**c**) 8-storey buildings ($T_{fb} = 0.4$, 0.6 and 0.8 s, respectively) equipped with different types of isolation systems

There is an apparent correlation between a_2 and a_3. The coefficient a_3 increases almost linearly with a_2, reaching a peak for values of the NL factor of the order of 0.6–0.65, independently from the value of T_l/T_{fb}. For NL > 0.65 the coefficient a_3 rapidly tends to zero.

In order to reduce the computational efforts to find simple analytical expressions of a_2 and a_3, LRB/HDRB and FPB/SB + LDRB isolation systems have been examined separately (see Table 2), focusing the attention on the data corresponding to 0.15 < NL < 0.65. As stated

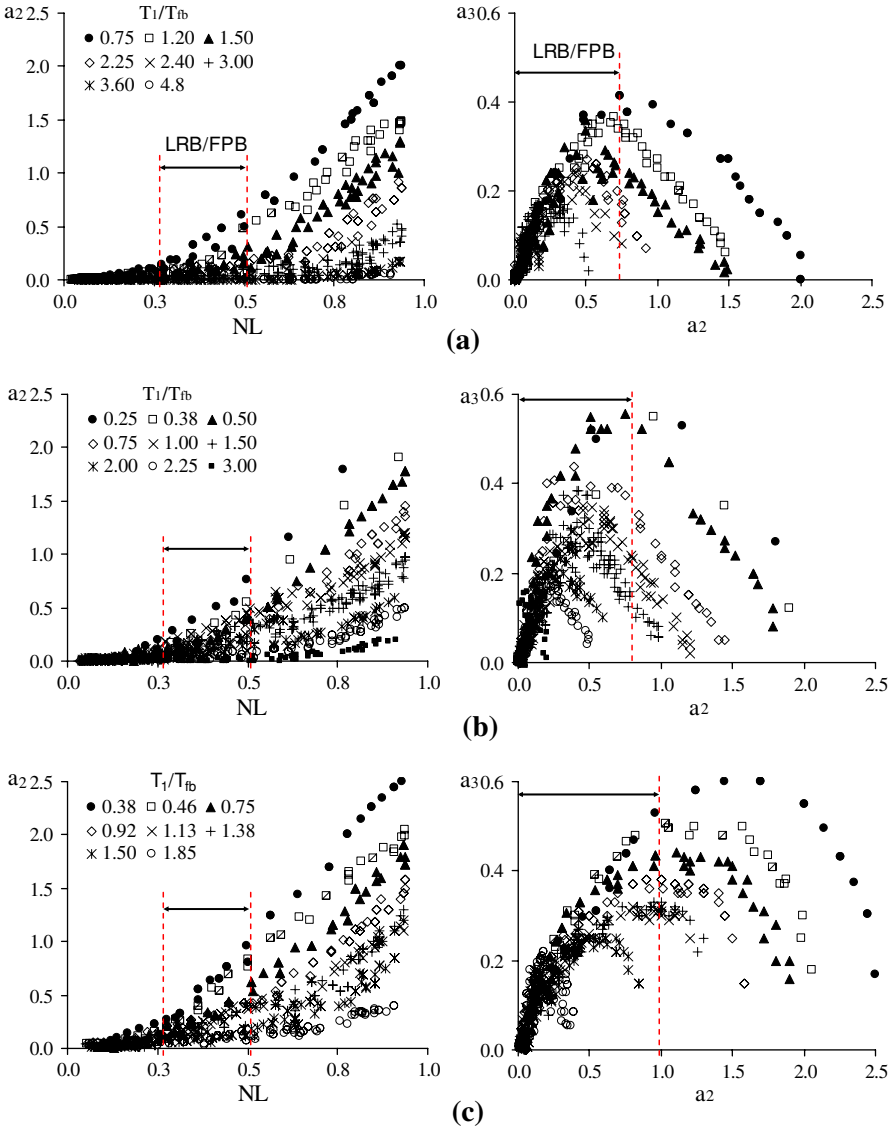

Fig. 9 (**a**) 3-storeys, (**b**) 5-storeys and (**c**) 8-storeys BI-buildings equipped with bilinear IS's (EPH model of Fig. 1): (left) Trend of the coefficient a_2 as a function of the NL factor for different period ratios T_1/T_{fb} and (right) correlation between the coefficients a_2 and a_3

above, this range largely cover the typical values of NL associated to the two types of IS herein considered (see Table 1).

6.1.1 Analytical expressions for LRB/HDRB isolation systems

A two stage regression analysis has been carried out to derive the analytical expression of a_2 and a_3 for LRB/HDRB isolation systems.

Table 3 Parameters governing the analytical expression of a_2 for buildings with LRB/HDRB isolation systems

Storeys	m	p	q	r
3	0.3–0.1 T_1/T_{fb} (valid for $T_1/T_{fb} < 3$)	2.5	0.5	2.0
5	0.7–0.3 T_1/T_{fb} (valid for $T_1/T_{fb} < 2.3$)	2.5	0.5	2.0
8	1.0–0.5 T_1/T_{fb} (valid for $T_1/T_{fb} < 2$)	2.5	0.5	2.0

In the first stage of the analysis, a change of variables (more precisely a scale distortion of the X- and Y-axis, with respect to the graphical representation of a_2 shown in Fig. 9) has been carried out, to get a linear formulation of the problem. Two auxiliary variables have been defined:

$$X_{EPH} = \frac{NL^p}{\left(\frac{T_{is}}{T_{fb}}\right)^q} \tag{19}$$

$$Y_{EPH} = \frac{a_2}{\left(\frac{T_{is}}{T_{fb}}\right)^r} \tag{20}$$

where "p", "q" and "r" are three numerical parameters which do not depend on the number of storeys of the building. The optimal values of "p", "q" and "r" are reported in Table 3, along with the angular coefficients "m" of the straight lines.

In the diagrams on the left-hand side of Fig. 10, the data set relevant to LRB/HDRB isolation systems are displayed in the new graphical format. As can be observed, the data points lie along straight lines passing through the origin, whose inclination depends on the period ratio T_1/T_{fb} and the number of storeys of the building. The slope of the regression lines becomes steeper as soon as T_1/T_{fb} reduces. The R-square coefficient (R^2) associated to each regression line varies between 0.92 and 0.99, thus proving the good fit of the obtained relations. It is worth to note that, for the 3- and 5-storey buildings, the number of regression lines shown in the diagrams is less than the number of permutations of T_1/T_{fb} considered ($3T_1 \times 2T_{fb} = 6T_1/T_{fb}$). This is partly due to the recurrence of some combinations of T_1/T_{fb} and partly to the attainment of limit values of T_1/T_{fb} for which a_2 is practically zero over the considered range of NL.

In the second stage of the analysis, the angular coefficients "m" derived in the first stage of the analysis have been regressed as a function of T_1/T_{fb}, separately for each prototype building. The fitting curves of the angular coefficients "m" are shown, together with the associated R^2, in the small diagrams inside the above discussed ones in Fig. 10. The linear equations expressing "m" as a function of T_1/T_{fb} are reported in Table 3, for each prototype building. The range of validity of each equation is also reported. In essence, the equations are cut off as soon as the angular coefficient becomes zero.

The analytical expression of a_2 can be represented in explicit form by simply rearranging the linear relations previously derived:

$$a_2 = m \cdot NL^p \cdot \left(\frac{T_{is}}{T_{fb}}\right)^{(r-q)} \tag{21}$$

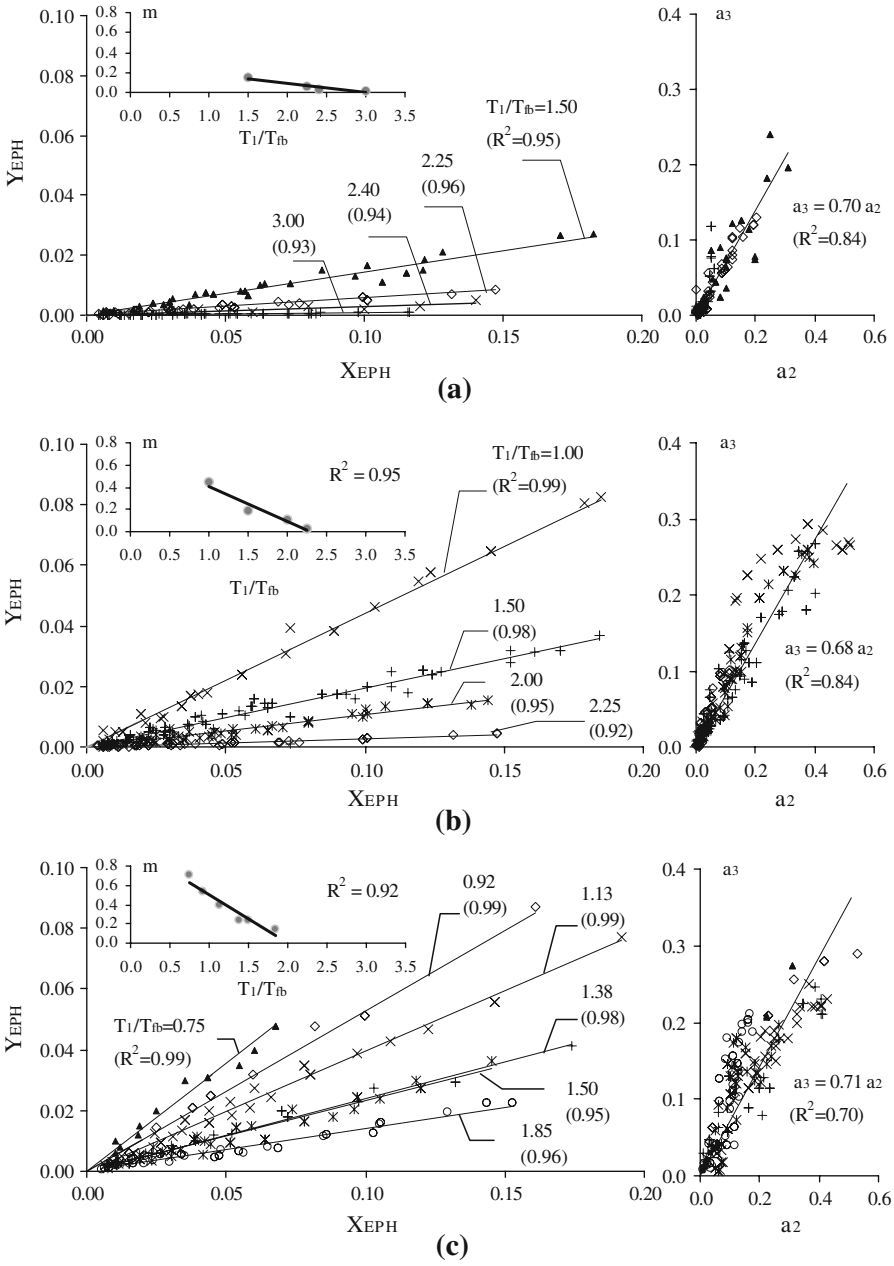

Fig. 10 (left) Regression analysis of a_2 and (right) correlation a_2 versus a_3 for (**a**) 3-storeys, (**b**) 5-storeys and (**c**) 8-storeys buildings with LRB/HDRB isolation systems

The expression of a_2 given before is valid for $0.15 < NL < 0.65$. For $NL < 0.15$, both a_2 and a_3 can be assumed equal to zero. For buildings with 4, 6 or 7 storeys, linear interpolation of the "m" values of Table 3 can be accepted.

The diagrams on the right hand-side of Fig. 10 show the correlation between a_2 and a_3. A linear relationship, with R^2 in the range 0.7–0.84, is found. It can be expressed, independently from the number of storeys, as follows:

$$a_3 = 0.7 \cdot a_2 \tag{22}$$

It is worth to note that the proposed relations (see Eqs. 21 and 22) satisfy the boundary conditions, since both a_2 and a_3 tend to zero as soon as either NL or T_1/T_{fb} tends to a given limit value.

6.1.2 Analytical expressions for FPB/SB+LDRB isolation systems

A two-stage regression analysis procedure has been followed also for FPB/SB + LDRB isolation systems. The same auxiliary variables have been preliminary defined (see Eqs. 19 and 20) and the same functional form of a_2 has been then obtained (see Eq. 21). Obviously, different values of "m", "p", "q" and "r" have been found (see Table 4). The main difference with respect to the LRB/HDRB isolation systems is the negligible dependency of a_2 from T_1/T_{fb}, which indeed has no physical relevance for the IS under consideration. The aforesaid remark is confirmed by Fig. 11a, which shows the fitting curves to the set of data derived from NTHA results. As can be observed, all the data points (regardless their period ratio T_1/T_{fb}) line up along three straight lines passing through the origin, whose inclination depends on the number of storeys of the building only. The values of the angular coefficient "m" are listed in Table 4, for each prototype building. It is worth to note that the values of m are linearly correlated to the number of storeys ($m = 0.08 \cdot N + 0.68$ with $R^2 = 0.99$). For buildings

Table 4 Parameters governing the analytical expression of a_2 for buildings with FPB/SB+LDRB isolation systems

Storeys	m	p	q	r
3	0.90	1.50	1.80	2.10
5	1.10	1.50	1.80	2.10
8	1.30	1.50	1.80	2.10

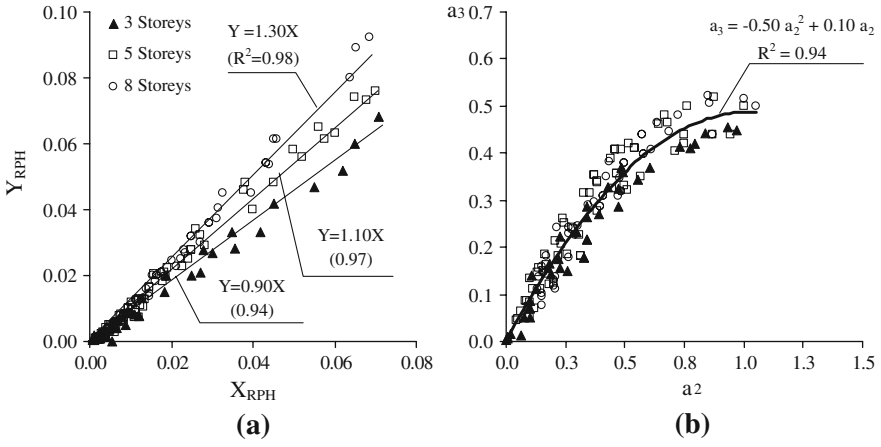

Fig. 11 (**a**) Regression analysis of a_2. (**b**) correlation between a_2 and a_3 for buildings with FPB/SB + LDRB isolation systems

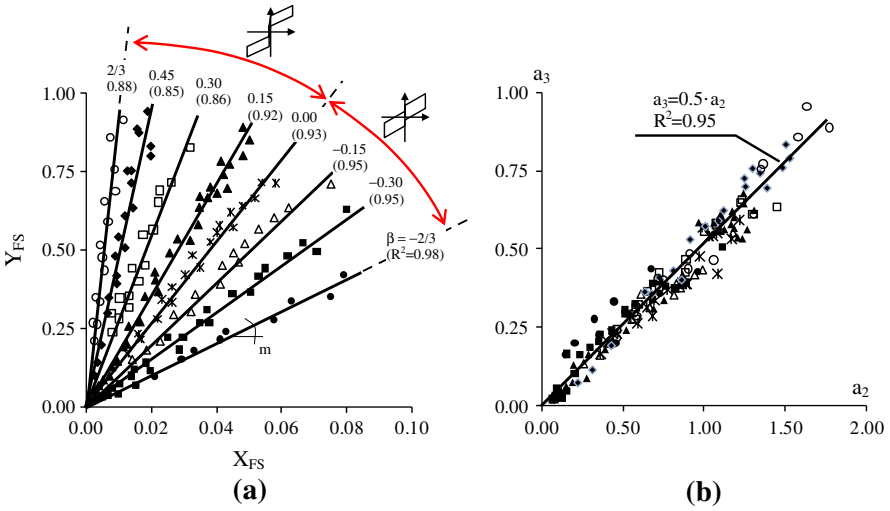

Fig. 12 (**a**) Regression analysis of a_2 and (**b**) correlation between a_2 and a_3 for buildings with SB + SMA isolation systems

with a number of storey equal to 4, 6 or 7, therefore, a linear interpolation of the values of "m" reported in Table 4 can be carried out. The coefficient a_3 can be expressed as a function of a_2 by means of the following parabolic relationship (see Fig. 11b):

$$a_3 = a_2 \cdot (1 - 0.5 \cdot a_2) \tag{23}$$

6.2 Isolation systems with double Flag-Shaped cyclic behaviour

Figure 12 shows the scatter plot of the data relevant to the SB + SMA isolation system, in the modified $X_{FS} - Y_{FS}$ plane. The filters applied to the data of Fig. 12 are those relevant to the isolation ratio T_{is}/T_{fb} ($\geq$2.0), effective period of vibration T_{is} ($\leq$4 s) and maximum displacement capacity D_u (<350 mm). No filter to the NL factor has been applied.

The same auxiliary variables defined before (see Eqs. 19 and 20) have been adopted. As a consequence, the same functional form of a_2 (see Eq. 21) has been obtained. In this case, however, the optimal values of the coefficients "q" and "r" practically coincides, thus eliminating the dependence of a_2 from the isolation ratio T_{is}/T_{fb}. The optimal value of the coefficient "p" can be assumed approximately equal to 2.

As can be observed in Fig. 12a, all the data points, derived from NTHA results, line up along straight lines passing through the origin, whose inclination depends on the strength ratio β (see Eq. 9) only. The angular coefficient (m) of the regression lines of Fig. 12a, indeed, can be expressed as a function of the strength ratio β through the following hyperbolic law (see Fig. 13):

$$m = \frac{30.4}{\left(2.4 - (\beta + 1)^{1.2}\right)^{2.75}} \tag{24}$$

which has been derived with the last squares method.

The coefficient a_3 turns out to be linearly correlated to a_2 (see Fig. 12b), in accordance with the following relationship:

$$a_3 = 0.5 \cdot a_2 \tag{25}$$

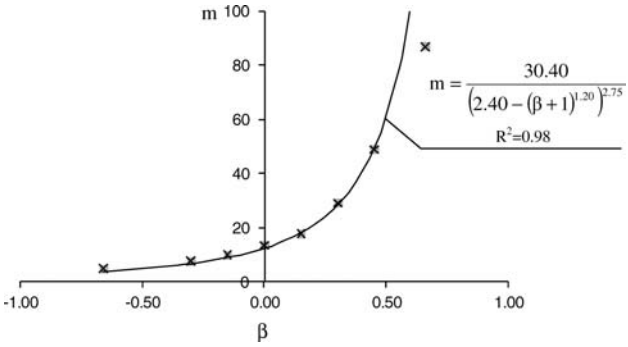

Fig. 13 Regression analysis of the angular coefficient "m" (see Fig. 12) for buildings with SB + SMA IS's

For SB + SMA isolation systems, therefore, the coefficients a_2 and a_3 do not depend either on the number of storeys of the building or on the period ratios T_1/T_{fb} and T_2/T_1, at least in the period ranges examined in this study (see Table 2). The coefficients a_2 and a_3 (hence the higher-mode contributions to the proposed lateral force distributions) significantly increase with the strength ratio β and (for a given β) with the NL factor. Both a_2 and a_3 tend to zero when NL tends to zero.

7 Application and verification of the proposed approach

The proposed 3-M method has been developed by expressing the "displacement" profile of the structure (Δ_i in Eq. 7) as a linear combination of the first three approximate modal shapes of the BI-building (see Eq. 18), in which the coefficients of combination depend on the main IS parameters (NL, T_1/T_{fb}, T_{is}/T_{fb} and β, precisely).

The LSA of BI-buildings is mainly performed with the scope of evaluating maximum stresses (and displacements) in the superstructure. At the beginning of the LSA, indeed, the isolation system is completely defined, having been designed based on the response of an equivalent SDOF system. From the appropriate response spectrum the design values of the base shear (V_b) and IS displacement (D_d), as well as the effective period of vibration of the BI-building, are drawn. The main differences between force-based and displacement-based design method are relevant to the characteristics of the equivalent SDOF system and to the target parameters selected at the beginning of design. The LSA of BI-buildings is carried out on a MDOF model of the structure with the IS modelled through its effective stiffness at the design displacement. According to the proposed approach, the following step-by-step procedure should be followed when LSA is performed:

Step 1: Determine the fundamental period of the superstructure in the fixed-base configuration (T_{fb}). If modal analysis results are not available, reference can be carried out to the approximate equations recommended by some seismic codes (e.g. see Eqs. 14 and 14').

Step 2: Evaluate the elastic (T_1), post-elastic (T_2) and effective (T_{is}) periods of vibration of the BI-structure, modelling the BI-building as a lumped-mass linear SDOF system, with stiffness equal to k_1, k_2 and k_{is}, respectively (see Fig. 1).

Step 3: Calculate the period ratios T_1/T_{fb}, T_2/T_1 and T_{is}/T_{fb}.

Step 4: Derive the approximate modal shapes (ϕ_{ji}) of the BI-building from Eqs. 10 and 11, with the IS modelled through its effective stiffness (k_{is}) at the design displacement (D_d).

Step 5: Calculate the non-linearity factor NL of the IS at its design displacement (D_d). The general expression of the NL factor given in Eq. 4 can be specialized to each type of IS's considered in this study as follows:

$$NL = \frac{(\alpha - 1) \cdot (1 - \alpha)}{\mu \cdot [1 + \alpha \cdot (\mu - 1)]} \quad \text{for LRB/HDRB} \tag{26}$$

$$NL = \frac{\mu_{FR}}{\mu_{FR} + \frac{D_d}{R_c}} \quad \text{for FPB} \tag{27}$$

$$NL = \frac{\mu_{FR}}{\mu_{FR} + \frac{k_r \cdot D_d}{W}} \quad \text{for SB+LDRB} \tag{28}$$

$$NL = \frac{1}{1 + \frac{F_2^*}{\mu_{FR} \cdot W}} \quad \text{for SB} + \text{SMA} \tag{29}$$

where:
$\mu = D_d/D_y$ is the ductility ratio,
$\alpha = (T_2/T_1)^{-0.5}$ is the post-yield hardening ratio,
μ_{FR} is the friction coefficient of the sliding bearings,
R_c is the radius of curvature of FPB,
k_r is the elastic stiffness of LDRB,
W is the total weight of the building (base floor included),
F_2^* is the force of SMA at the design displacement D_d.

Step 6: (e.g. for bilinear hysteretic IS's): Using Eq. 20, with the values of "m", "p", "q" and "r" listed in Tables 3 and 4, determine a_2 based on the values of T_1/T_{fb}, T_{is}/T_{fb} and NL derived in step 3 and 5, respectively. Alternatively, the charts shown in Fig. 14 can be used. The charts of Fig. 14 are the graphical representation of Eq. 21, valid for LRB/HDRB and FPB/SB + LDRB isolation systems: a_2 is obtained entering a proper graph (identified by the number of storeys of the building) with a given value of $NL^p \cdot (T_{is}/T_{fb})^{r-q}$ to intercept the line associated to a given value of T_1/T_{fb}. For Flag-Shaped IS's a similar procedure can be outlined (see Sect. 6.2.).

Step 7: Determine a_3 from Eqs. 22, 23 and 25.

Step 8: Evaluate the "displacement" profile of the BI-building (Δ_i^*) from Eq. 18, using the approximate modal shapes derived in step 4 and the values of a_2 and a_3 obtained in step 6–7.

Step 9: Distribute the design base shear (V_b) along the height of the building according to Eq. 7, in proportion to storey masses m_i and corresponding storey "displacements" Δ_i^*, to get the equivalent static lateral forces (F_i) for LSA.

Step 10: Perform a LSA of the superstructure and compute the design forces of the structural members.

The step-by-step procedure described before can be applied to low-to-medium rise frame buildings ($T_{fb} \leq 0.8$ s), with floor mass and storey stiffness values almost uniform over the height of the structure. The only requirements for the IS are: (i) NL < 0.65, (ii) $T_{is}/T_{fb} > 2.0$ and (iii) $T_{is} < 4.0$ s.

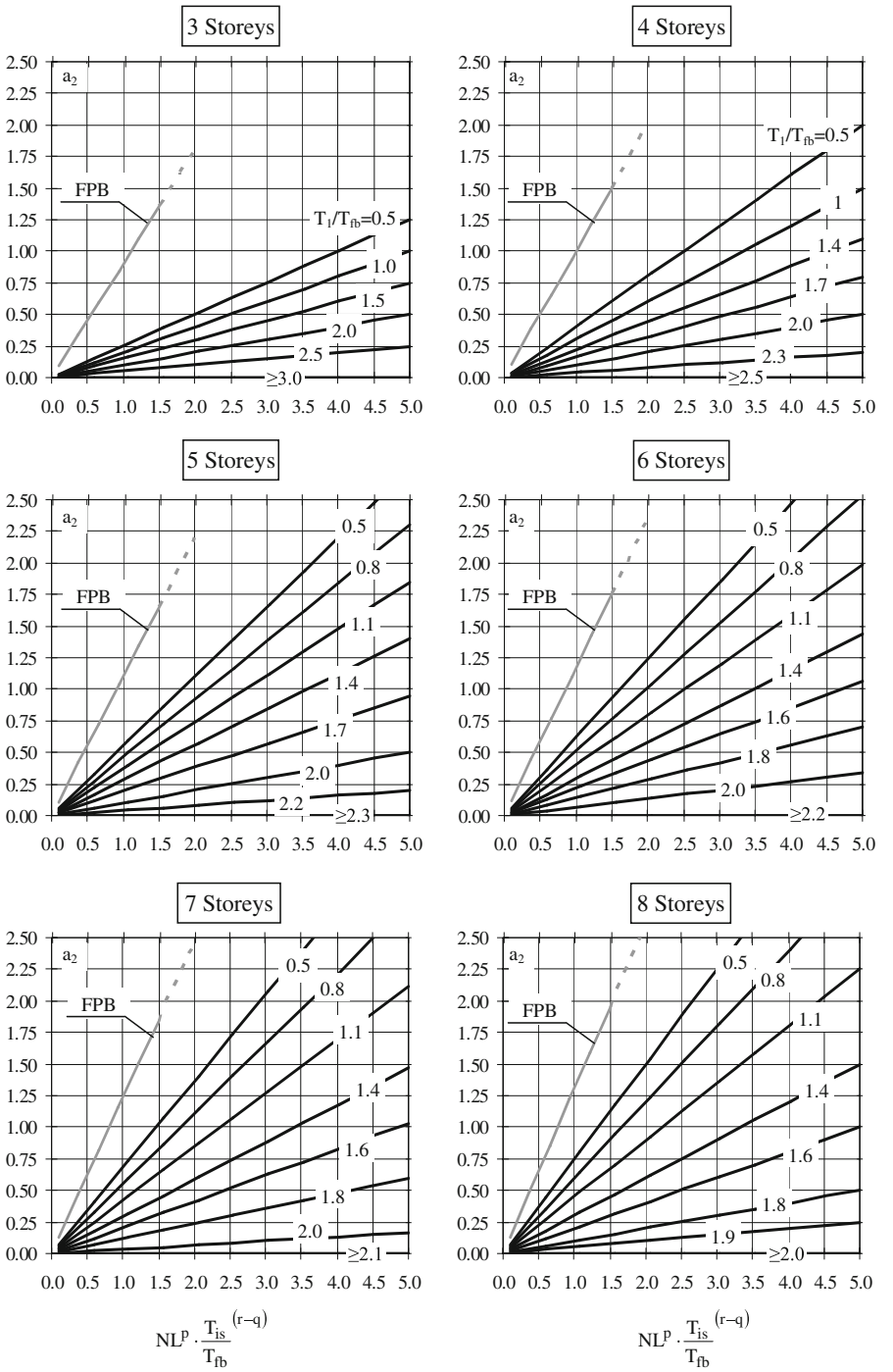

Fig. 14 Charts for the graphical evaluation of a_2 for multi-storeys (N = 3 − 8) BI-buildings, equipped with LRB/HDRB or FPB/SB + LDRB isolation systems

It should be noted that the base shear V_b, obtained from RSA of the equivalent SDOF system, includes only the effects of the first mode of vibration of the BI-structure. This is adequate for determining the required shear capacity of the IS. The lateral force distributions proposed in this study, however, directly account for the effects of the higher modes. There is no need to apply any dynamic amplification factor to approximately consider the potential increase in the design forces due to higher mode effects (Priestley et al. 2007). On the other hand, the variability of the IS mechanical behaviour with air temperature, loading rate and magnitude of vertical load, as well as the changes in the IS mechanical properties due to ageing and differences within the same production lot, should be considered in the analysis. In accordance with some seismic codes (e.g. Eurocode 8; CEN 1998), this can be carried out by performing an upper and lower bound analysis, assuming the most unfavourable IS characteristics for accelerations and IS displacements, respectively. Generally speaking, accelerations and inertia forces induced by the earthquake should be evaluated taking into account the maximum expected value of effective stiffness and the minimum expected value of effective damping and friction coefficient (upper bound analysis). Conversely, IS displacements should be evaluated taking into account the minimum expected value of effective stiffness, effective damping and friction coefficient (lower bound analysis). Using prearranged distributions of equivalent static force (like those provided by the current seismic codes), therefore, the LSA of the building should be performed only for the upper bound analysis, in which a higher base shear is attained. Following the proposed approach, on the contrary, the LSA of the building should be performed during both analyses, as the equivalent static force distribution changes with the IS parameters (NL, T_{is}/T_{fb}, T_1/T_{fb} and T_2/T_{fb}).

Figure 15 compares some typical normalized ($V_b = 1$) storey-shear envelopes derived from NTHA with the corresponding storey-shear profiles obtained from LSA, using the proposed 3-MM lateral force distributions with $V_b = 1$. For comparison, in the diagrams of Fig. 15, the storey-shear profiles obtained from LSA, using uniform and inverted-triangular lateral force distributions, are also reported. The comparison is carried out, separately, for (a) 3-storey, (b) 5-storey and (c) 8-storey buildings, equipped with different LRB, FPB and SB+SMA isolation systems. The selected IS configurations refer to typical values of NL for each IS type (see Table 1). The IS parameters remain almost the same passing from one prototype building to another. The IS configurations considered in Fig. 15 are the same as those of Fig. 8.

The comparisons of Fig. 15 clearly point out the great accuracy of the proposed 3-M method, compared to that attained with the current seismic code-based LSA approaches (see uniform and inverted triangular distributions). Indeed, using the 3-MM lateral force distributions, the percent errors between NTHA and LSA storey shear-forces never exceed 5%, for all the cases of Fig. 15. More importantly, it is apparent that there is no constant dynamic amplification factor (Priestley et al. 2007) that can guarantee a degree of accuracy, over the entire height of the structure, case studies comparable to that of the proposed approach.

The aforesaid observations are substantiated by Table 5, which shows, for each IS type, the percentage of cases (over approximately 1500 case studies) in which the error between NTHA and LSA storey shear-forces fall within given percent ranges. Two different error indexes are considered in Table 5. The first index, named E_i, represents the error relevant to the ith level of the building:

$$E_i = \frac{V_i^{LSA} - V_i^{NTHA}}{V_i^{NTHA}} \tag{30}$$

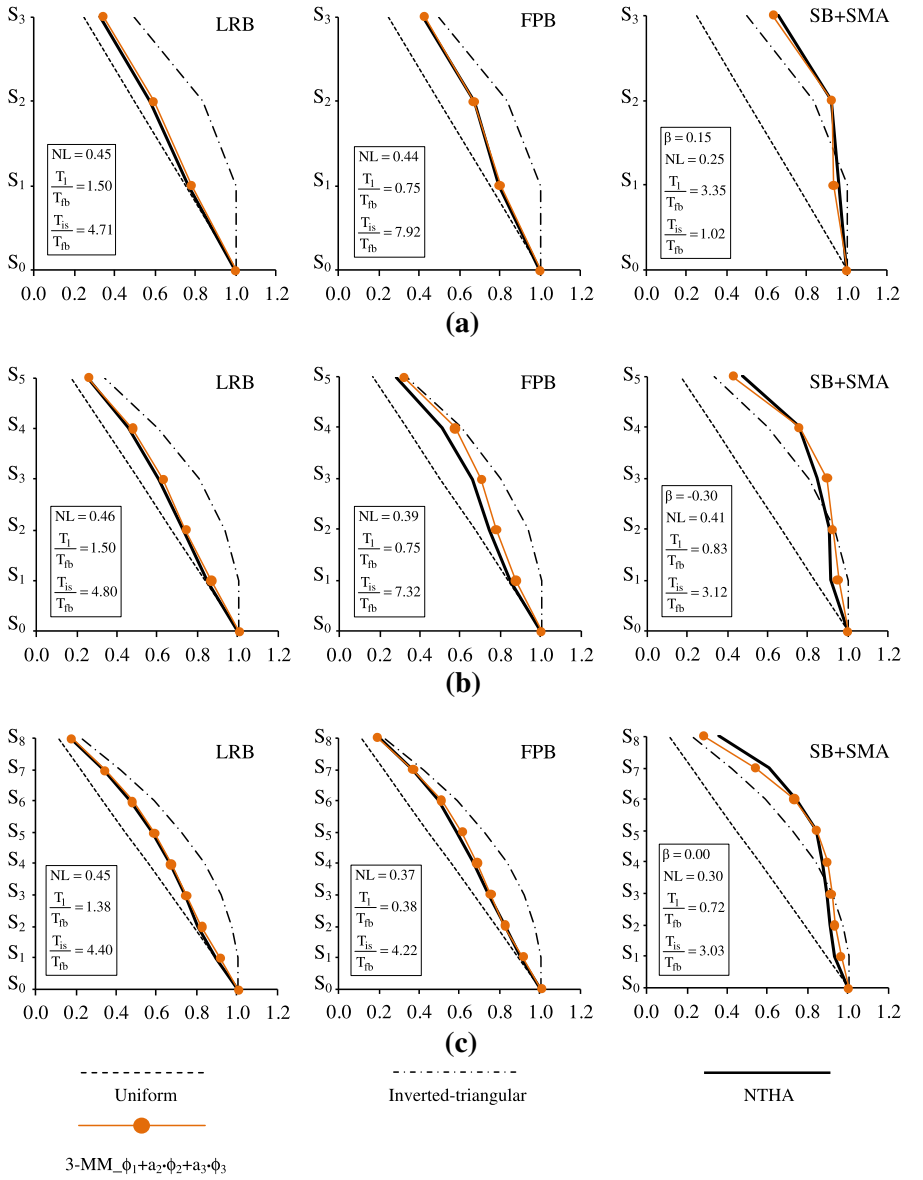

Fig. 15 Comparison between normalized ($V_b = 1$) storey-shear envelopes obtained from NTHA and corresponding storey-shear profiles obtained from LSA using the proposed lateral force distributions for (**a**) 3-storey, (**b**) 5-storey and (**c**) 8-storey buildings equipped with different IS types

Positive values of E_i mean that the LSA storey-shear overestimates the corresponding NTHA storey-shear.

The second index, indicated by MSE in Table 5, represents the mean standard error over all the storeys of the building:

Table 5 Percentage of cases (over approximately 1,500 analyses) in which the error at the *i*th level of the structure (E_i) and the mean standard error over all the storeys of the building (MSE) fall within given percent ranges

IS type	$-20\% \leq E_i < -10\%$	$-10\% \leq E_i < 0\%$	$0\% \leq E_i < 10\%$ ($0\% \leq$ MSE $< 10\%$)	$10\% \leq E_i$(MSE) $< 15\%$ ($10\% \leq$ MSE $< 15\%$)	$15\% \leq E_i$(MSE) $\leq 25\%$ ($15\% \leq$ MSE $< 25\%$)
LRB	1 %	14 %	83 %	1 %	1 %
HDRB			(97%)	(2%)	(1%)
FPB	0%	7 %	81 %	5 %	7 %
SB + LDRB			(76%)	(14%)	(10%)
SB + SMA	2 %	5 %	88 %	4 %	1 %
			(97%)	(3%)	(0%)

$$MSE = \sqrt{\frac{\sum_{i=1}^{N} E_i^2}{N}} \tag{31}$$

As can be observed, in approximately 5–15% of the cases, the error index E_i is between 0 and 10%, while in approximately 80–90% of the cases it is between −10% and 0%. Considering the MSE index, it can be noted that, for the LRB/HDRB and SB + SMA isolation systems, in some 97% of the cases, the MSE is less than 10%. A slightly worse degree of accuracy is observed for the FPB/SB + LDRB isolation system.

In Fig. 16 the storey shear distributions obtained through LSA, using different lateral force distributions (see Eqs. 1–3 and 5–7), are compared to those computed by NTHA. The comparison is carried out for the 5-storey building, endowed with two different IS's, whose mechanical characteristics are: (a) $F_y/W = 0.05$, $D_y \cong 5\,\text{mm}$, $T_1 = 0.6\,\text{s}$, $\alpha = 5\%$, $\mu \cong 30$ (corresponding to $\xi_{is} \cong 24\%$ and NL $\cong 0.38$) and (b) $F_y/W = 0.05$, $D_y = 10\,\text{mm}$, $T_1 = 0.9\text{s}$, $\alpha = 5\%$, $\mu \cong 20$ (corresponding to $\xi_{is} \cong 29\%$ and NL $\cong 0.46$). These IS parameters are fully compatible with those selected by other authors in their studies (Tsai et al. 2003; Ryan and York 2007; Andriono and Carr 1991b).

As can be observed in Fig. 16, the shear profiles obtained from LSA, using the lateral force distributions proposed by other authors, significantly differ from the NTHA results and the 3-MM lateral force distributions of this study. Such discrepancies can be basically ascribed to three main aspects: (i) different assumptions in the IS modelling, (ii) different criteria in the selection of the input ground motions and (iii) different approach in the examination of the NTHA results. In the studies by Tsai et al. (2003) and Lee et al. (2001), for instance, reference is made to an equivalent viscous-elastic model, which could be suitable for HDRB-IS (as explicitly recognized by the authors), but not for IS's characterised by a strong nonlinear behaviour or large values of the effective damping (e.g. LRB, FPB, etc.). The lateral force distribution proposed by Andriono and Carr (1991b), on the other hand, has been derived by examining the maximum seismic response of BI-buildings, with bilinear hysteretic IS's, generated by individual earthquake records. The lateral force distribution proposed by Ryan and York (2007), instead, has been obtained by examining the median values of the peak storey shear-forces generated by a suite of ground motions, whose response spectra did not match any target response spectrum. In the present study, on the contrary, reference has been made

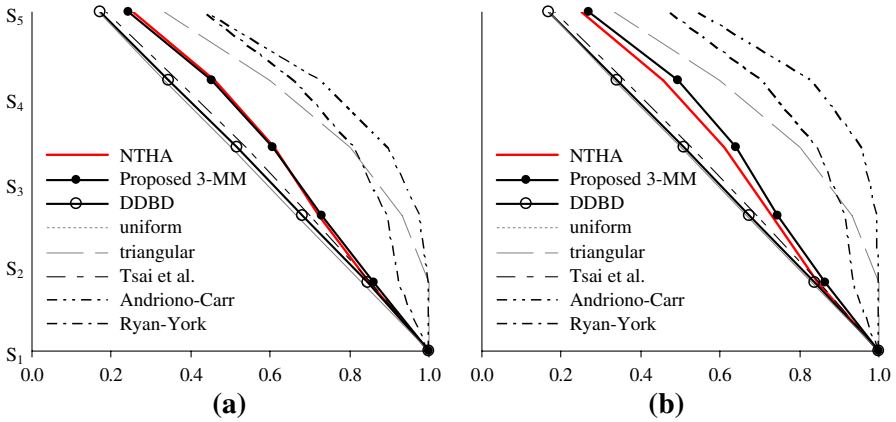

Fig. 16 Five-storey BI-building endowed with bilinear IS's characterised by (**a**) $F_y/W = 0.05.$, $D_y \cong 5\,mm$, $T_1 = 0.6\,s$, $\alpha = 5\%$, $\mu \cong 30$ (i.e. $\xi_{is} \cong 24\%$ and NL $\cong 0.38$) and (**b**) $F_y/W = 0.05.$, $D_y = 10\,mm$, $T_1 = 0.9\,s$, $\alpha = 5\%$, $\mu \cong 20$ (i.e. $\xi_{is} \cong 29\%$ and NL $\cong 0.46$). Comparisons of normalized storey shear distributions obtained from LSA using different lateral force distributions, including that proposed in this study

to the mean values of the peak storey shear-forces generated by a set of seven accelerograms compatible (on average) with a specified target response spectrum, as required by most of the current seismic codes (CEN 1998; ICBO 1997).

The lateral force distributions developed in this study, therefore, besides being perfectly in line with the DDBD approach, are also suitable for the implementation in the current force-based seismic design codes. This can be carried out within the LSA methods, by modelling the IS through its effective stiffness and effective damping at the design displacement (equivalent linear viscous-elastic behaviour). The use of lateral force distributions, that account for the higher mode contributions (like those derived in this study), may allow to extend the applicability of the LSA methods to many situations for which current seismic codes require the use of Nonlinear Time-History Analysis (CEN 1998; ASCE 2005).

8 Summary and conclusion

A new approach for the evaluation of accurate lateral force distributions for the Linear Static Analysis (LSA) of Base Isolated (BI-) Buildings has been presented. The proposed lateral force distribution F_i is proportional to the "displacement" profile Δ_i, which is expressed as a linear combination of the first three approximate modal shapes of the BI-building (see Eq. 18), with the IS modelled through its effective stiffness at the design displacement D_d. For this reason, the acronym 3-MM (3-Mode Method) has been used to identify the proposed method. The combination coefficients of the modal shapes are expressed as a function of a number of IS parameters, accounting for its actual nonlinear mechanical behaviour. The combination coefficients have been derived from the results of an extensive Nonlinear Time History Analyses (NTHA) investigation, carried out on 3-, 5- and 8-storey shear-type framed buildings, equipped with a variety of isolation systems, including: (i) Lead Rubber Bearings (LRB) and High Damping Rubber Bearings (HDRB), (ii) Friction Pendulum Bearings (FPB) and combinations of flat Sliding Bearings (SB) with Low-Damping Rubber Bearings (LDRB) and (iii) Combinations of flat SB and Shape Memory Alloys (SMA)-based re-centring devices.

Particular care has been taken in the selection of the IS characteristics for NTHA, in order to comply with the typical values of IS parameters adopted in the current practice.

Based on the comparisons between the storey-shear envelopes derived from NTHA and the corresponding storey-shear profiles obtained from LSA, using different lateral force distributions, the following considerations can be drawn:

(i) currently used lateral force distributions, that neglect (or consider roughly) the contribution of higher modes, can significantly underestimate (or overestimate) the seismic response of BI-buildings, in case of nonlinear IS's;
(ii) the storey-shear profiles predicted by the proposed 3-M method are in excellent agreement with those obtained from NTHA, throughout the height of the building (percent errors at the ith storey lower than 10% in most of the examined cases);
(iii) the proposed 3-M method is accurate even in circumstances under which the LSA code approaches cannot be applied, i.e. for buildings with more than 4–5 storeys equipped with IS's that cannot be modelled with an equivalent linear viscous-elastic behaviour.

This study clearly proves that accurate predictions from the LSA of BI-building with nonlinear IS's can be achieved only specialising the lateral force distributions to the IS characteristics. The proposed 3-M method is expected to be a suitable tool for the evaluation of realistic equivalent-static-forces for the analysis and design of BI-buildings. The use of the proposed 3-M method also gives the possibility to extend the applicability of the LSA to a greater number of situations.

In the current version, the proposed 3-M method can be applied to low-to-medium rise frame buildings ($T_{fb} \leq 0.8$ s) with floor mass and storey stiffness values almost uniform over the height of the structure. The only requirements of the IS are: (i) non-linearity factor NL (see Eq. 4) less than 0.65, (ii) isolation ratio T_{is}/T_{fb} greater than 2.0 and (iii) effective isolation period (T_{is}) lower than 4 s.

Further developments of the proposed 3-M method should include: (1) the examination of the influence of the beam-column stiffness ratio, which affects both the fundamental period of vibration and the modal shapes of frame buildings, (2) the examination of the validity of the method for different structural types (e.g. shear-wall systems) and (3) the verification of the limits of validity of the method for BI-buildings with non-uniform distribution of storey masses and/or storey stiffnesses over the height of the structure.

Acknowledgements This work has been carried out within the RELUIS 2005–2008 program, Project No. 4—"Development of displacement-based approaches for the seismic design and assessment of structures", funded by the Italian Civil Protection Department.

References

ALGA SpA, ALGA Brochure: Antiseismic devices. Milano, Italy. http://www.alga.it

Al-Hussaini TM, Zayas VA, Constantinou MC (1994) Seismic isolation of a multi-story frame structure using spherical sliding isolation systems. National Center for Earthquake Engineering Research, Technical Report No NCEER-94-0007, Buffalo, NY, USA

Andriono T, Carr AJ (1991) Reduction and distribution of lateral seismic inertia forces on base-isolated multi-storey structures. Bull NZ Natl Soc Earthq Eng 24(3):225–237

Andriono T, Carr AJ (1991) A simplified earthquake resistant design method for base-isolated multistorey structures. Bull NZ Natl Soc Earthq Eng 24(3):238–250

American Society of Civil Engineers (ASCE) (2005) ASCE SEI7-05: Minimum design loads for buildings and other structures. Reston, VA, 424 pp

Bertero RD, Bertero VV (2002) Performance-based seismic engineering: the need for a reliable conceptual comprehensive approach. Earth Eng Struct Dyn 31(3):627–652. doi:10.1002/eqe.146

Bridgestone, Multi-rubber bearings: seismic isolation system for buildings. Huntington Beach, CA, USA
Cardone D, Dolce M (2007) A displacement-based design procedure for buildings with seismic isolation. In: Proceedings third international conference on structural engineering, mechanics and computation, Cape Town, South Africa
Cardone D, Dolce M, Ponzo FC (2006) The behaviour of SMA isolation systems based on a full-scale release test. J Earthq Eng 16(5):1–28
Cardone D, Dolce M, Palermo G (2008) Direct displacement-based design of seismically isolated bridges. Bull Earthq Eng. doi:10.1007/s10518-008-9069-2
Casas JR, Jara M (2006) A direct displacement-based method for the seismic design of bridges on bilinear isolation devices. Eng Struct 28:869–879. doi:10.1016/j.engstruct.2005.10.016
CEN ENV-1-1 European Committee for Standardization (1998) Eurocode 8: design provisions for earthquake resistance of structures, part 1.1: general rules, seismic actions and rules for buildings
Chopra AK (1997) Dynamics of structures. Prentice Hall International Inc, London
Constantinou M, Mokha A, Reinhorn AM (1990) PTFE bearings in base isolation: modelling. J Earthq Eng 116(2):455–472
Constantinou MC, Winters CW, Theodossiou D (1993) Evaluation of SEAOC/UBC analysis procedures. Part 2: flexible superstructure. In: Proceedings ATC-17-1 seminar on seismic isolation, passive energy dissipation and active control, San Francisco, CA, USA
DIS—Dynamic Isolation Systems Inc DIS Brochure: seismic isolation for buildings and bridges. 885 Denmark Dr, suite 101, Nevada, USA. http://www.dis-inc.com
Decreto Ministero delle Infrastrutture 14.01.2008 (DMI) (2008) Approval of the new technical standards for constructions (in Italian). GU no 29 4-2-2008—Suppl. Ordinario no 30, Roma
Dolce M, Cardone D, Marnetto R (2000) Implementation and testing of passive control devices based on shape memory alloys. Earth Eng Struct Dyn 29:945–968. doi:10.1002/1096-9845(200007)29:7<945::AID-EQE958>3.0.CO;2-#
Dolce M, Cardone D, Croatto F (2005) Frictional behaviour of steel-PTFE interfaces for seismic isolation. Bull Earthq Eng 3(1):75–99. doi:10.1007/s10518-005-0187-9
Dolce M, Cardone D, Ponzo FC (2007) Shaking-table tests on reinforced concrete frames with different isolation systems. Earth Eng Struct Dyn 36(5):573–596. doi:10.1002/eqe.642
Faccioli E, Paolucci R, Rey J (2004) Displacement spectra for long periods. Earthq Spectra 20(2):347–376
Fenz D, Constantinou MC (2006) Behaviour of double concave friction pendulum bearings. Earthq Eng Struct Dyn 35(11):1403–1424. doi:10.1002/eqe.589
Fenz DM, Constantinou MC (2007a) Spherical sliding isolation bearings with adaptive behavior: theory. Earthq Eng Struct Dyn 37(2):163–183. doi:10.1002/eqe.751
Fenz DM, Constantinou MC (2007b) Spherical sliding isolation bearings with adaptive behavior: experimental verification. Earthq Eng Struct Dyn 37(2):185–205. doi:10.1002/eqe.750
GB50011 (2001) Code for seismic design of buildings. China Building Industry Press, Beijing, China (in Chinese)
Higashino M, Okamoto S (2006) Response control and seismic isolation of buildings. Taylor & Francis, Ltd, UK
Highway Innovative Technology Evaluation Center (HITEC) (1998) Evaluation findings for skellerup base isolation elastometric bearings. Report No 98–30063, ISBN 0-7844-0376-7, USA
International Conference of Buildings Officials (ICBO) (1997) UBC: earthquake regulations for seismic-isolated structures, USA
International Code Council (ICC) (2000) IBC: chap 16: seismically isolated structures, USA
Industriale FIP SpA, FIP Brochure: seismic devices—data sheets. Padova, Italy. http://www.fip-group.it
Jangid RS (2007) Optimum lead-rubber isolation bearings for near-fault motions. Eng Struct 29(6):2503–2513. doi:10.1016/j.engstruct.2006.12.010
Kelly TE (1992) Skellerup industries lead rubber isolation bearings: experimental properties. Holmes Consulting Group Ltd, New Zealand
Kelly TE (2001) Base isolation of structures: design guidelines. Holmes Consulting Group Ltd, New Zealand
Kowalsky MJ (2002) A displacement-based approach for the seismic design of continuous concrete bridges. Earth Eng Struct Dyn 31:719–747. doi:10.1002/eqe.150
Lee DG, Hong JM, Kim J (2001) Vertical distribuition of equivalent static loads for base isolated building structures. Eng Struct 23:1293–1306. doi:10.1016/S0141-0296(01)00031-1
Mokha A, Constantinou M, Reinhorn AM (1990) PTFE bearings in base isolation: testing. J Earthq Eng 116(2):438–454
Ministry of Vehicle Infrastructure and Transport (MVIT) (2001) Guidelines for calculation procedure and technical standard on seismically isolated structures, Japan
Naeim F, Kelly JM (1999) Design of seismic isolated structures. John Wiley & Sons, Inc, New York

NEHRP (1997) Federal emergency management agency (FEMA-273): guidelines for the seismic rehabilitation of buildings, USA

Pettinga D, Priestley MJN (2005) Dynamic behaviour of reinforced concrete frames designed with direct displacement-based design. J Earthq Eng 9:309–330. doi:10.1142/S1363246905002419

Pietra D, Calvi GM, Pinho R (2008) Displacement-based seismic design of isolated bridges. Research Report ROSE-2008/01, IUSS Press, Pavia, Italy

Priestley MJN (1993) Myths and fallacies in earthquake engineering—conflicts between design and reality. Bull NZ Natl Soc Earthq Eng 26(3):329–341

Priestley MJN (2003) Myths and fallacies in earthquake engineering, revisited. IUSS Press, Pavia, Italy

Priestley MJN, Calvi GM, Kowalsky MJ (2007) Displacement-based seismic design of structures. IUSS Press, Pavia, Italy

Robinson WH (1982) Lead-rubber hysteretic bearings suitable for protecting structures during earthquakes. Earth Eng Strut Dyn 10:593–604. doi:10.1002/eqe.4290100408

Ryan KL, Chopra AK (2004) Estimation of seismic demands on isolators based on nonlinear analysis. J Struct Eng 30(3):392–402. doi:10.1061/(ASCE)0733-9445(2004)130:3(392)

Ryan KL, York K (2007) Vertical distribution of seismic forces for simplified design of base-isolated buildings. ASCE Structures Congress, Long Beach, CA, USA

SAP2000 Inc (2004) (Berkeley, CA, USA): static and dynamic finite element analysis of structures

Scheller J, Constantinou MC (1999) Response history analysis of structures with seismic isolation and energy dissipation systems: verication examples for Program SAP2000. Multidisciplinary Center for Earthquake Engineering Research, Report No MCEER 99–02, Buffalo, New York, USA

Skinner RI, Robinson WH, Mc Verry GH (1993) An introduction to seismic isolation. John Wiley & Sons Ltd, Chichester, West Sussex, UK

Sullivan TJ, Priestley MJN, Calvi GM (2005) Development of an innovative seismic design procedure for frame-wall structures. J Earthq Eng 9:279–307. doi:10.1142/S1363246905002407

TIS SpA TIS Brochure: High damping rubber isolators. Roma, Italy. http://www.tis.it

Tsai CS, Chen BJ, Chiang TC (2003) Experimental and computational verification of reasonable design formulae for base-isolated structures. Earthq Eng Struct Dyn 32:1389–1406. doi:10.1002/eqe.279

Winters CW, Constantinou MC (1993) Evaluation of static and response spectrum analysis procedures of SEAOC/UBC for seismic isolated structures. Technical Report NCEER-93-0004, National Center for Earthquake Engineering Research, Buffalo, NY, USA